ELECTRONIC SUPPORTING INFORMATION

All in one porous material: Exceptional sorption and selective sensing of hexavalent chromium by a Zr^{4+} MOF

Sofia Rapti,[a]† Debajit Sarma,[b,c]† Stavros A. Diamantis,[d] Euaggelia Skliri,[e] Gerasimos S. Armatas,[e] Athanassios C. Tsipis,[a] Youssef S. Hassan,[f] Mohamed Alkordi,[f] Christos D. Malliakas,[b] Mercouri G. Kanatzidis,[b] Theodore Lazarides*,[d] John C. Plakatouras*,[a] and Manolis J. Manos*,[a]

[a.] *Department of Chemistry, University of Ioannina, 45110 Ioannina, Greece.*
[b.] *Department of Chemistry, Northwestern University, Evanston, IL 60208.*
[c.] *Department of Chemistry, Indian Institute of Technology, Patna, Bihta - 801103, India*
[d.] *Department of Chemistry, Aristotle University of Thessaloniki, 54124 Thessaloniki, Greece.*
[e.] *Department of Materials Science and Technology, University of Crete 71003 Heraklion, Greece.*
[f.] *Center for Materials Science, 6th of October, Zewail City of Science and Technology, Giza, 12588 Egypt*

Contents *Page*

EXPERIMENTAL SECTION

Materials. $ZrCl_4$, 2-aminoterephthalic (NH_2-H_2BDC), 2-pyridinecarboxaldeyde and $NaBH_4$ were purchased from Aldrich. The solvents were used as received.

SYNTHESES

2-((pyridin-2-ylmethyl)amino)-terephthalic acid. 2-pyridinecarboxaldeyde (0.884 g, 8.25 mmol) was added into a stirred suspension of NH_2-H_2BDC (1 g, 5.5 mmol) in MeOH (70 mL), in a 100 mL single-neck round-bottomed flask. Within a few minutes a clear yellow solution was formed. To this solution, solid $NaBH_4$ (2.08g, 55 mmol) was gradually added. The resulting mixture was stirred for 2 h. A colorless solid was precipitated and isolated by filtration, washed with MeOH and dried in the air. The product 2-((pyridin-2-ylmethyl)amino)-terephthalic acid obtained was used for the synthesis of **MOR-2** without further treatment. Yield: 1 g

^{1}H NMR (500 MHz, DMSO-d_6): δ (ppm) 13.00 (2H, br, COOH), 9.73 (1H, t, J = 6 Hz, -NH-), 8.49 (1H, d, J = 5 Hz, pyH), 7.71 (1H, d, J = 7.5 Hz, pyH), 7.68 (1H, dd, J_1 = 8 Hz, J_2 = 7.5 Hz, PyH), 7.31 (1H, d, J = 8 Hz, ArH), 7.20 (1H, dd, J_1 = 8 Hz, J_2 = 5 Hz, pyH), 6,99 (1H, s, ArH), 6.93 (1H, d, J = 8 Hz, ArH), 4.40 (2H, d, J = 6 Hz, -CH_2-); **^{13}C NMR** (500 MHz, DMSO-d_6): δ (ppm) 172.81, 171.19, 161.00, 149.36, 149.34, 136.96, 131.12, 122.17, 122.07, 121.15, 115.63, 111.42, 49.00.

MOR-2. $ZrCl_4$ (0.625g, 2.7 mmol) and 2-((pyridin-2-ylmethyl)amino)-terephthalic acid (1.017, 0.374 mmol) were dissolved in 75mL DMF and 5mL HCl in a jar. The jar was sealed and placed

in an oven operated at 120 ˚C, remained undisturbed at this temperature for 20 h and then was allowed to cool at room temperature. Pale yellow powder (no protonated **MOR-2**) was isolated by filtration and dried in the air. This product was treated with 4 M HCl solution to afford the **MOR-2** material. Yield: 1 g. **MOR-2** was analyzed as $H_{16}[Zr_6O_{16}(H_2PATP)_4]Cl_8{\cdot}12H_2O$. Anal. Calc. (%) for $C_{56}H_{88}Cl_8N_8O_{44}Zr_6$: C, 27.93; H, 3.68; N, 4.65; Zr, 22.73. Found (%): C, 27.95; H, 3.21; N, 4.64; Zr, 22.64. EDS analysis for **MOR-2** indicated Zr:Cl molar ratio = 1:1.30 (calculated ratio=6:8=1:1.33).

^{1}H NMR (400 MHz, D_2O-H_2SO_4): δ (ppm) 8.25 (1H, d, pyH), 8.14 (1H, m, pyH), 7.65 (2H, d, ArH+pyH), 7.54 (1H, m, pyH), 6.92 (1H, d, ArH), 6.67 (1H, s, ArH), 4.62 (2H, s, -CH_2-).

MOR-2-HA composite. 0.100 g of sodium alginate (SA) was dissolved in 200 mL of water. A fine suspension of **MOR-2**-SA was formed by adding 1 g of **MOR-2** to ~ 20 ml of the SA solution. To this suspension, HCl solution (final concentration ~ 4 M) was then added with continuous stirring. The composite **MOR-2-HA** immediately precipitated and was isolated by filtration. The product was further treated with 4M HCl acid to ensure complete protonation of the functional groups of the material. Yield: 0.885 g. EDS analysis for **MOR-2-HA** indicated Zr:Cl molar ratio =1:1.3. PXRD indicated the similarity between **MOR-2-HA** and **MOR-2** (see below).

ANALYTICAL AND CHARACTERIZATION TECHNIQUES

Elemental analyses (C, H, N, Zr). C,H,N analyses were performed by the in-house facilities of the University of Science and Technology, Center for Materials Science, Zewail City of Science and Technology, Giza, Egypt. Zr was determined gravimetrically as ZrO_2. Specifically, **MOR-2** sample **(**100 mg**)** was heated at ~ 800 ^{0}C in air for ~12 h. **MOR-2** was fully converted to ZrO_2 (as confirmed by PXRD). The amount of ZrO_2 produced was then accurately weighted. The

measurement was performed in triplicate and the results were then averaged to determine the % Zr content of **MOR-2**.

In house X-ray powder diffraction. Powder X-ray diffraction of the samples were measured at room temperature on a STOE-STADIMP powder diffractometer equipped with an asymmetric curved Germanium monochromator (CuKα1 radiation, λ = 1.54056 Å) and one-dimensional silicon strip detector (MYTHEN2 1K from DECTRIS). The line focused Cu X-ray tube was operated at 40 kV and 40 mA. Powder of each sample was packed in a 1 mm diameter polyimide capillary (polymer substrate with neither Bragg reflections nor broad peaks above 10 degrees) and measured in Debye-Scherrer geometry on a spinning stage (~ 200 rpm). Intensity data from 3 to 125 degrees two theta were collected over a period of 17 h with a step of 0.005 degrees. Instrument was calibrated against a NIST Silicon standard (640d) prior the measurement.

PDF experiment. Powder of sample was packed in a Kapton capillary (1 mm diameter) and diffraction data were collected at room temperature using the rapid acquisition pair distribution function (RA-PDF) technique.[1] Data were collected using a Perkin-Elmer image plate detector and 60 keV energy X-rays (λ= 0.2114 Å) at the 11-ID-C beam line at APS. Accumulation of 200 frames with an exposure time of 2 s per frame was used to improve counting statistics. The data were integrated using the program FIT2D.[2] Various corrections were made to the data, such as subtraction of background and container, Compton and fluorescence scattering, geometric corrections, absorption, etc.[3] using the program PDFgetX2.[4] Finally, the normalized data were truncated at 25 $Å^{-1}$ before the PDF was calculated. Simulations were carried out using PDFfit2 and PDFgui.[5] Crystallographic models obtained by Rietveld analysis were used as starting models for the refinement of the PDF data. Scaling factor, unit cell parameters, coordinates, and isotropic thermal factors were freely refined in the PDF refinement using the *I4/m* space group.

The pair distribution function method (PDF) is a powerful technique for local structure studies. PDF describes the distribution of interatomic distances in a material. The power and the difference of PDF from other crystallographic techniques like Rietveld is that PDF is a total scattering technique which means both the Bragg and diffuse scattering are treated on an equal basis. PDF studies both the long-range atomic structure (Bragg reflections) and the local structure imperfections (diffuse component of the diffraction pattern). The data analysis does not presume any periodicity therefore the PDF technique is very useful for examining amorphous and crystalline samples.

The experiments are straightforward X-ray (or neutron) powder diffraction measurements. From the coherent part, $I^{coh}(Q)$, of the measured total diffracted intensity of the material we find the total scattering structure function, $S(Q)$

$$S(Q) = \frac{I^{coh}(Q) - \sum c_i \left| f_i(Q) \right|^2}{\left| \sum c_i f_i(Q) \right|^2} + 1 \qquad (1)$$

where the coherent intensity is corrected for background and other experimental effects and normalized by the flux and number of atoms in the sample. Here, c_i and f_i are the atomic concentration and X-ray atomic form factor, respectively, for the atomic species of type *i*. Momentum transfer, *Q*, is given by

$$Q = 4\pi \sin \vartheta / \lambda \qquad (2)$$

By Fourier transforming the expression $Q[S(Q)-1]$ we have

$$G(r) = (2/\pi) \int_{Q=0}^{Q_{\max}} Q[S(Q) - 1] \sin(Q \cdot r) dQ \qquad (3)$$

where $G(r)$ is the atomic pair distribution function which is also defined as

$$G(r) = 4\pi \cdot r[\rho(r) - \rho_0] \quad (4)$$

where ρ_0 is the average atomic number density, $\rho(r)$ is the atomic pair-density and r is a radial distance. The function $G(r)$ gives information about the number of atoms in a spherical shell of unit thickness at a distance r from a reference atom.

Finally, the experimental $G(r)$ can be compared and refined against a theoretical $G(r)$ from a structural model given by

$$G(r) + 4\pi \cdot r \cdot \rho_0 = \frac{1}{r}\sum_{\nu}\sum_{\mu}\frac{f(0)_\nu f(0)_\mu}{\langle f(0)\rangle^2}\delta(r - r_{\nu\mu}) \quad (5)$$

IR spectroscopy. IR spectra were recorded on KBr pellets in the 4000-400 cm^{-1} range using a Perkin-Elmer Spectrum GX spectrometer.

Thermal analyses. Thermogravimetric analyses (TGA) were performed on a NETZSCH STA 449Csystem. Thermal analysis was conducted from 25 to 600 or 700^oC in air atmosphere (100 mL min^{-1} flow rate) with a heating rate of 10 ^oC min^{-1}.

^{1}HNMR. ^{1}H NMR spectra were measured with Bruker 250 and 400 MHz spectrometers.

Energy dispersive spectroscopy (EDS) analyses. These measurements were performed on a JEOL JSM-6390LV scanning electron microscope (SEM) equipped with an Oxford INCA PentaFET-x3 energy dispersive X-ray spectroscopy (EDS) detector. Data acquisition was performed with an accelerating voltage of 20 kV and 120 s accumulation time.

FE-SEM. Scanning electron microscopy (SEM) images were taken with a field emission JEOL JSM 7000F electron microscope operating at 15 kV accelerated voltage. The samples were sputter-coated with a 5-10 nm Au film to reduce charging.

X-ray photoelectron spectroscopy (XPS). XPS measurements were performed on a Perkin Elmer Phi 5400 ESCA system equipped with a Mg Kα x-ray source. Samples were analyzed at pressures between 10^{-9} and 10^{-8} Torr with a pass energy of 29.35 eV and a take-off angle of 45°. All peaks were referred to the signature C_{1s} peak for adventitious carbon at 284.6 eV. Fitting of the peaks has been made by using the "Avantage" software (Thermo Scientific).

Gas sorption measurements.N_2 adsorption-desorption isotherms were measured at 77 K on a Quantachrome Nova 3200*e* sorption analyzer. Before analysis, all samples were EtOH-exchanged, activated via supercritical CO_2 drying and then, degassed at 120 ^oC under vacuum ($<10^{-5}$ Torr) for 12 h.The specific surface areas were calculated by applying the Brumauer-Emmett-Teller (BET) methodto the branch of isotherms in the 0.05–0.25 relative pressure (P/P_o) range. CO_2 adsorption isotherms were measured at 273 K using an IGA-003 gravimetric sorption analyzer (Hiden Isochema, UK). The activation of the materials was done as with the N_2 sorption measurements. The pore size distribution plot was obtained from the CO_2 adsorption data using the density functional theory (DFT) method.

Solid state UV/Vis. Solid stateUV/Vis spectra were obtained on a Shimadzu 1200 PC in the wavelength range of 200-800 nm.$BaSO_4$ powder was used as a reference (100% reflectance) and base material on which the powder sample was coated. The reflectance data were converted to absorption using the Kubelka-Munk function.[6]

Fluorescence spectra-sensing experiments. The fluorescence spectra were measured on a Hitachi F7000 spectrofluorometer. The light source was a Xenon arch lamp and the detector a red sensitive Hamamatsu R928 photomultiplyer tube. All spectra are corrected for instrument response using the correction function generated after calibration of the instrument with a standard light source. Appropriate long pass filters were used to remove scattering from the

sample and the monochromators. For the Cr(VI) sensing experiments, 1 mg of the MOF in the form of a fine powder were suspended in 10 ml of the respective medium (doubly distilled water or potable water) the pH of which was previously adjusted to 3 by careful addition of 4M HCl. The system was sonicated for 30 min and 1 mL was removed and placed in a luminescence quartz cuvette. Aliquots of $K_2Cr_2O_7$ 10^{-4} M (dissolved in the same medium as the MOF) were added using a precision Hamilton microsyringe (50 μL range) in order to achieve the desired Cr(VI) concentration. In the cases where real samples were used, stock solutions were prepared by diluting the samples to achieve a concentration of 10^{-4} M (measured by the UV-vis absorption at 350 nm, ε = 3300 $M^{-1}cm^{-1}$ at pH~3). Emission spectra were recorded 2 min after each addition. The emission spectrum after each addition was recorded three times to ensure signal stability.

Cr(VI) analyses by UV/Vis. UV/Vis solution spectra were also obtained on a Shimadzu 1200 PC in the wavelength range of 200-800 nm. Moderate to high concentrations (from 2 to several hundreds of ppm) of Cr(VI) were determined based on the characteristic UV-Vis absorption peaks of dichromate and chromate anions at 350 (ε =3300 $M^{-1}cm^{-1}$, pH~3) and 370 (ε =4200 $M^{-1}cm^{-1}$, pH~7) nm respectively.[7] Low Cr(VI) concentrations (0.05-2 ppm) were analyzed with the diphenylcarbazide (DPC) method.[7,8]The method is based on the formation of Cr(III)-diphenylcarbazone resulted from the oxidation of diphenylcarbazide by Cr(VI) in acidic medium (pH~1). The cationic Cr(III) complex has a red-violet color and strongly absorbs in the visible region (λ_{max} = 545 nm, ε =39600 $M^{-1}cm^{-1}$). The calibration curve obtained with the DPC method is shown in Figure S0. It can be seen that Cr(VI) can be analysed accurately well below 50 ppb with the DPC method (in fact the quantification limit for Cr(VI) was reported to be as low as 10 ppb[9]). Total Cr can be also determined by oxidizing any Cr^{3+} by $KMnO_4$.[7,8]

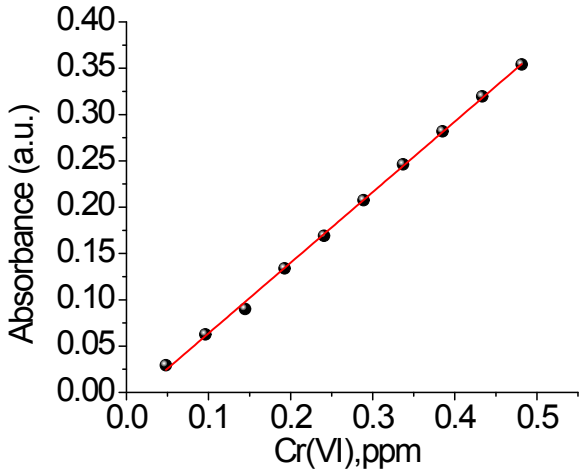

Figure S0. The calibration curve obtained with the DPC method (R^2=0.998).

Inductively Coupled Plasma-Mass Spectroscopy (ICP-MS). The Cr analyses for solutions with extremely low Cr content (<50 ppb) were performed by ICP-MS, specifically using a computer-controlled Thermo Scientific iCAP Q ICP-MS with a quadruple setup equipped with Collision Cell Technology. Isotope ^{52}Cr was analyzed. Nine standards of Cr in the range of 1-200 ppb were prepared by diluting commercial (Aldrich chemicals) 1000 ppm solution. All samples (including standards and a blank solution) were prepared in a 3% ultra pure HNO_3 solution with 2 ppb ^{89}Y and ^{115}In internal standards in order to correct for instrumental drift and matrix effects during analysis.[10] The quantification limit for Cr achieved with our ICP-MS analytical procedure was 0.1-0.3 ppb.

ION EXCHANGE STUDIES

Preparation of the column. 50 or 100 mg of **MOR-2-HA** composite and 5 g of sand (50-70 mesh SiO_2) was mixed in a mortar and pestle and filled in a glass column (0.7 cm ID column). Prior the ion exchange studies, the column was washed with ~ 7 mL HCl (4 M) solution and deionized water.

Batch ion-exchange studies. A typical ion-exchange experiment of **MOR-2** with $Cr_2O_7^{2-}$ is the following: In a solution of $K_2Cr_2O_7$ (0.4 mmol) in water (10 mL, pH ~ 3), compound **MOR-2**(100 mg, ~ 0.04 mmol of **MOR-2**) was added as a solid. The mixture was kept under magnetic stirring for ~5 min. Then, the polycrystalline material, which had orange-brown color, was isolated by filtration, washed several times with water and acetone and dried in the air. EDS analysis indicated no Cl in the exchanged product and presence of Cr. In order to determine the Zr:Cr ratio with accuracy, ICP-MS analysis has been performed on a sample digested in hot aqua regia. This analysis indicated a Zr:Cr ratio of ~ 0.7 (close to that calculated based on the isotherm sorption data, i.e. Zr:Cr =6:8=0.75). The EDS peaks for pristine vs. dichromate exchanged material are shown in the following graph:

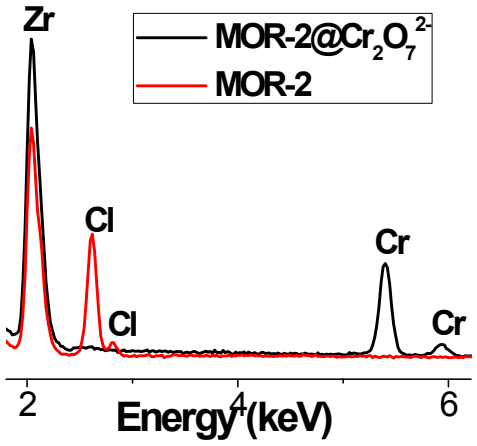

The isolation of the CrO_4^{2-} exchanged product was done similarly as that of the $Cr_2O_7^{2-}$ loaded material, with the exception that K_2CrO_4 was used instead of $K_2Cr_2O_7$. EDS also revealed no Cl for this exchanged material and presence of Cr. The Zr:Cr ratio determined by ICP-MS (on a sample digested in hot aqua regia) was ~ 1 (as expected based on the isotherm sorption data).

The Cr(VI) uptake from solutions of various concentrations was studied by the batch method at *V*:*m* ~ 1000 mL/g, room temperature and 1 h contact. These data were used for the determination

of Cr(VI) sorption isotherms. The competitive and variable pH ion exchange experiments were also carried out with the batch method at *V*: *m* ratio ~ 1000 mL/g, room temperature and 1 h contact. The batch ion exchange experiments with the potable and chrome plating solutions were also conducted with *V*: *m* ratio ~ 1000 mL/g, room temperature and 1 h contact. However, in the case of the batch ion exchange experiments with the original chrome plating sample B, the optimum Cr removal efficiency was achieved with *V*: *m* ratio ~ 500 mL/g.

For the determination of the sorption kinetics, Cr(VI) ion-exchange experiments of various reaction times (1-60 min) have been performed. For each experiment, a 10 mL sample of $Cr_2O_7^{2-}$ or CrO_4^{2-} solution (initial dichromate concentration = 21.6 ppm, pH~3;initial chromate concentration = 11.6ppm, pH~7) was added to each vial (containing 10 mg of **MOR-2** or **MOR-2-HA**) and the mixtures were kept under magnetic stirring for the designated reaction times. The suspensions from the various reactions were filtrated and the resulting solutions were analyzed for their chromium content with UV-Vis (DPC method) or ICP-MS.

Column Ion-Exchange studies

Several bed volumes of the solution were passed through the column and collected at the bottom in glass vials. The solutions were analyzed with UV-Vis or ICP-MS. The regeneration of the column was performed by its treatment with ~ 7 mL of HCl acid (4 M) solution. Then, the column is washed with enough water to remove excess acid. Column containing only sand as stationary phase showed no Cr(VI) sorption capacity.

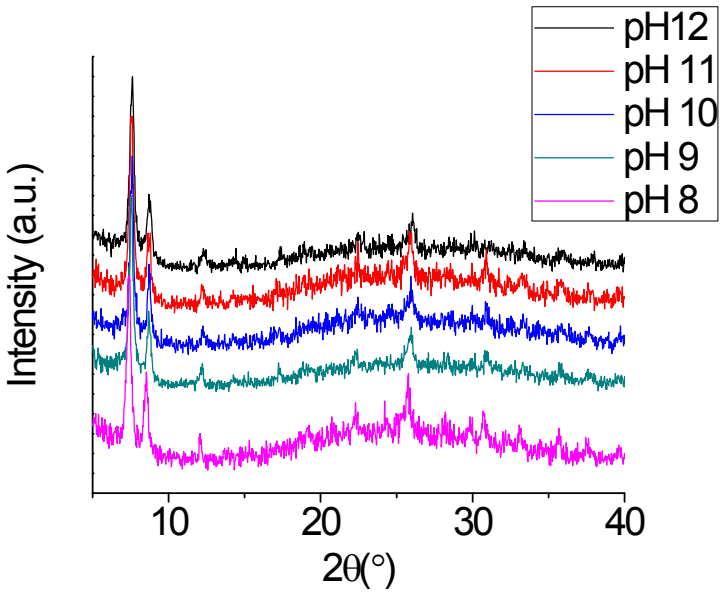

Figure S1. PXRD patterns of **MOR-2** after its treatment with alkaline water solutions (pH~8-12).

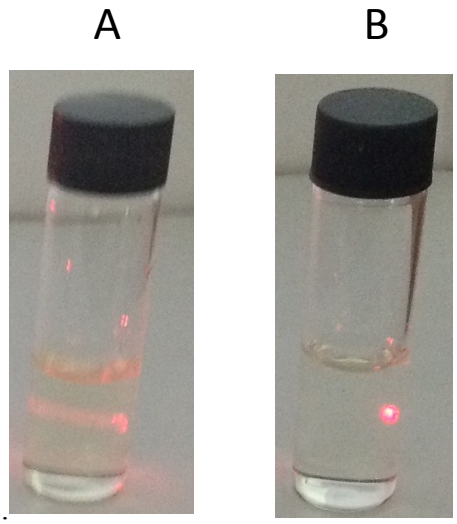

Figure S2. A. As **MOR-2**/sand column is washed with deionized water, **MOR-2** flows out of the column. It forms a fine suspension as confirmed by the test with the laser beam (Tyndall effect). B. By washing the **MOR-2-HA**/sand column with deionized water, the effluent collected is a clear solution (as proved by the test with the laser beam).

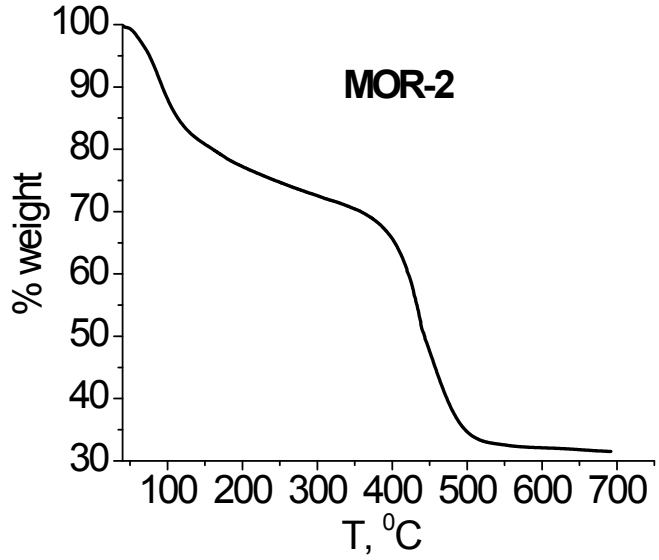

Figure S3. The TGA data for **MOR-2** measured in air. The **MOR-2** is finally transformed to ZrO_2 according to the equation

$[Zr_6O_8(H_2O)_4(H_2PATP)_4]Cl_8{\cdot}xH_2O \rightarrow 6ZrO_2$+ volatile products ($CO_2$, H_2O, HCl, NO_xetc).

Thus, one mole of $[Zr_6O_4(OH)_8(H_2O)_4(H_2PATP)_4]Cl_8{\cdot}xH_2O$ yields 6 moles of ZrO_2 or molecular weight (g) of $[Zr_6O_4(OH)_8(H_2O)_4(H_2PATP)_4]Cl_8{\cdot}xH_2O$ (= 2192.11+18x) yields 6 × molecular weight (g) of ZrO_2 (6 × 123.2 = 739.2) .

From the TGA data, we know that 100 g of **MOR-2** are converted to 31.5 g of ZrO_2. Thus, **MOR-2**/ZrO_2 mass ratio = 100/31.5= 3.175 or 2192.11+18x/739.2 = 3.175 and x ~ 9. This number of lattice water molecules is relatively close to that (12 lattice H_2O molecules) found from the elemental (C,H, N, Zr) analyses data. In addition, the % Zr value calculated from the TGA data (specifically from the mass of the ZrO_2 residue) is 23.31 %, which is also relatively close to that found from the Zr gravimetric analyses (22.64 %).

Crystal Structures of MOR-2, MOR-2@$Cr_2O_7^{2-}$, and MOR-2@CrO_4^{2-}

The crystal structures of the pristine material and the Cr(VI) loaded materials were solved by X-ray Powder Diffraction methods, refined with Rietveld methods, and confirmed by PDF (Pair Distribution Function) experiments.

The X-ray powder pattern of **MOR-2** was indexed with TREOR leading to a tetragonal cell, with approximate dimensions 14.7, 14.7, and 20.8 Å (Fig. S4). Bearing in mind that the unit cell can be transformed to a cubic cell, (see for example Fig. S5) and the face centered cubic cell of UiO-66, the best candidate space group must be a body centered one. Eventually I4/m was selected as described below.

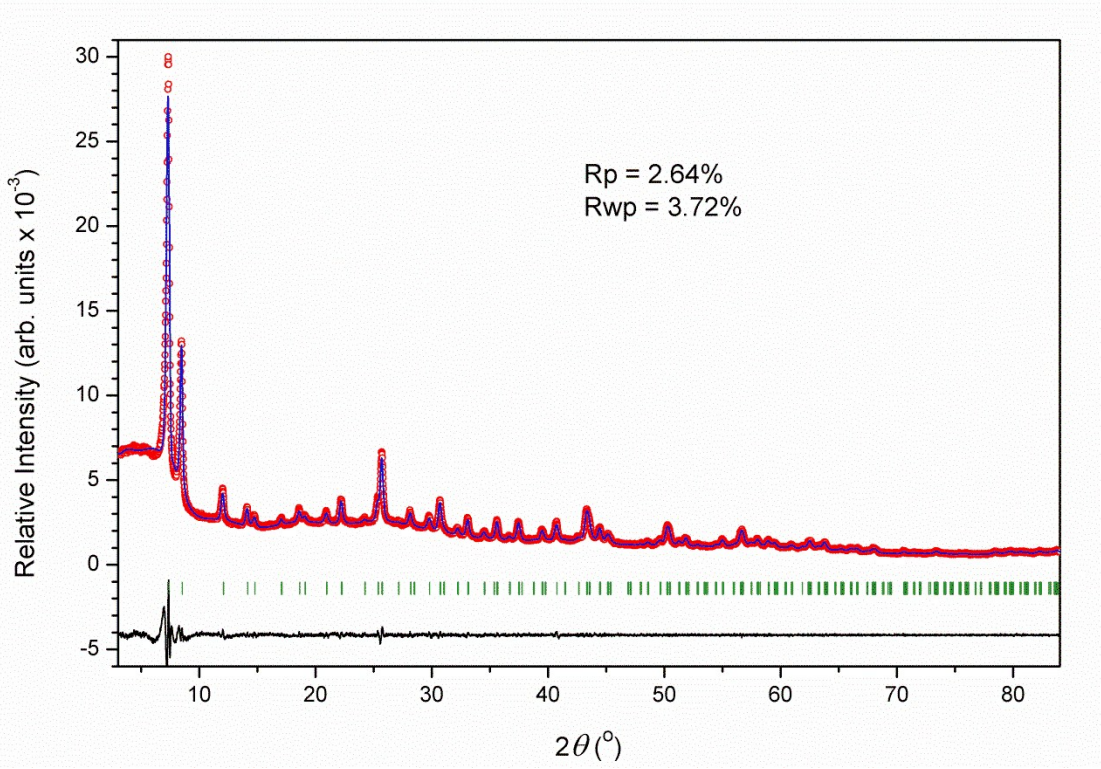

Figure S4. Structureless pattern profile refinement plot of **MOR-2** (space group: *I4/m*) (λ_{CuKa} = 1.54056). Red: experimental points; blue: calculated points; green: Bragg peaks; black: difference pattern (exp.-calc.).

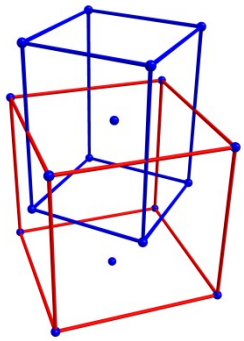

Figure S5. Body centered tetragonal (blue) vs. face centered cubic (red) cell in UiO-66. Blue spheres represent the Zr_6O_8 core.

Attempts to solve the structure with direct methods (EXPO 2014, reference 27 in main text) resulted in solutions with the Zr_6O_8 core on anticipated positions for quite a few space groups (namely $P4_2$, $I\bar{4}$, I4/m, I4/mmm). There was much electron density all over the cell which could not be assigned to familiar shapes (i.e. hexagons). The best solution from direct methods was introduced to Materials Studio where the ligand was built.

The space group selection problem was dealt with trying to describe as realistic as possible the anticipated positional disordering of substituted 2-pyridinemethylamino group on position 2 of the terephthalate moiety (Fig. S6). Additionally, second harmonic generation (SHG) experiments suggested a centrosymmetric structure, so non centrosymmetric space groups were ignored.

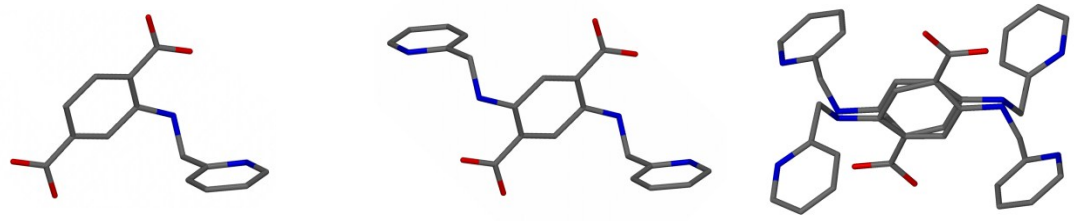

(a) (b) (c)

Figure S6. Appearance of the ligand in miscellaneous space groups: a) $I\bar{4}$, b) I4/m, c) I4/mmm. Inversion centers are located on the centroids of the benzene ring in (b) and (c).

Finally, I4/m was selected, since the limited disordering would allowed reduced calculation cost and relatively easier study of the produced structure solutions.

Analytical data for **MOR-2** suggested a Zr_6O_8:ligand ratio of 1/4, or Zr:ligand, 3/2. Our first approach to the solution of the structure was to build a 12-connected network based on UiO-66 and solve and refine the structure considering that has a defected UiO-66 structure, using partial occupancies for the ligand molecules, as done previously (see reference 25j in main text). All of those attempts were met with failure. The next step was to build an 8-connected network, i.e. remove the four linkers about the equatorial plane of the Zr_6O_8 core (Fig. S7).

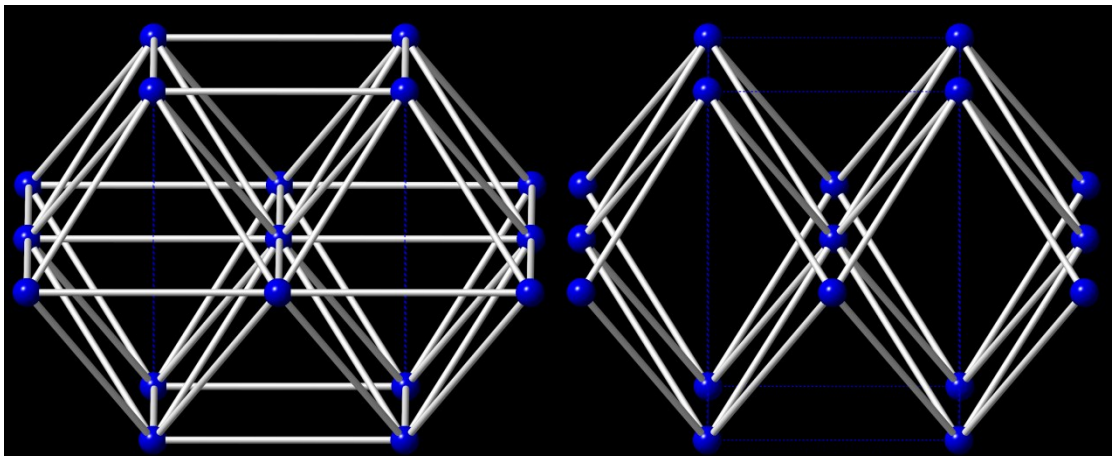

(a) (b)

Figure S7. Transformation of a 12-connected node (a) to an 8-connected node (b) embedded in a body centered tetragonal lattice.

This way a realistic model of the structure was produced which allowed Rietveld refinement (Fig. S8). The crystallographic data are given in pages S19-S21. In Fig. S9, the interactions of the guest Cl^- anions and functional group of the H_2PATP ligand with the Zr_6 core are shown.

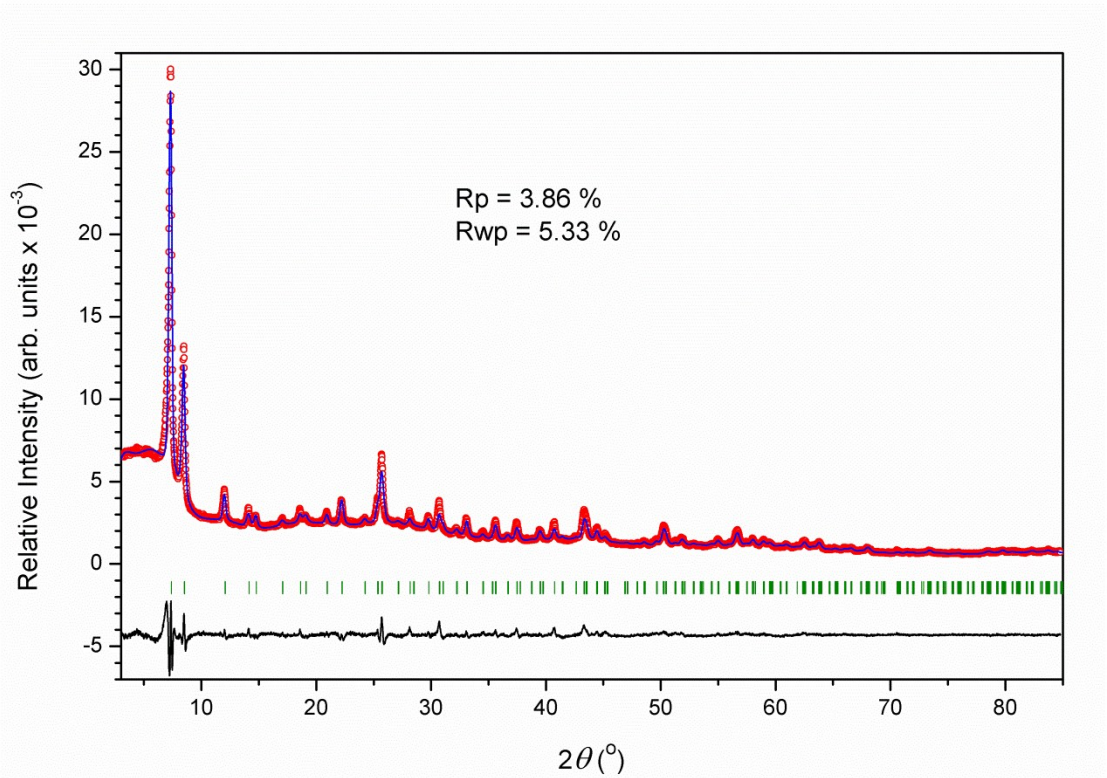

Figure S8. Rietveld plot of **MOR-2.** Red: experimental points; blue: calculated points; green: Bragg peaks; black: difference pattern (exp. – calc.).

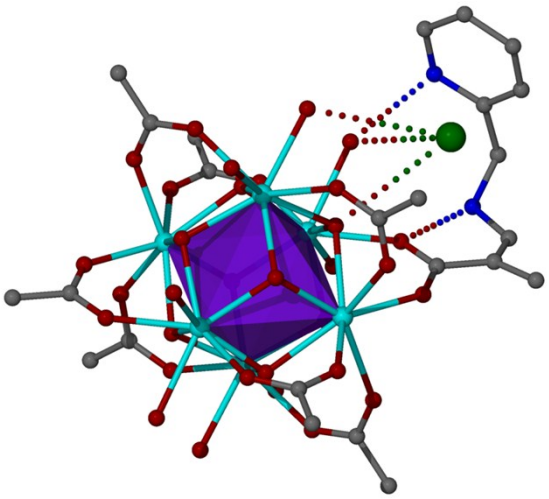

Figure S9. The connectivity of the Zr_6O_8 core in **MOR-2** showing the interactions of the counter ion and the ligand's substituted group with the core. Color code: Zr, sky blue; O, red; C, grey; N, blue; Cl, green.

data_**MOR-2**
_audit_creation_date 2017-04-02
_audit_creation_method 'Materials Studio'
_symmetry_space_group_name_H-M *'I4/m'*
_symmetry_Int_Tables_number 87
_symmetry_cell_setting tetragonal
loop_
_symmetry_equiv_pos_as_xyz
x,y,z
-x,-y,z
-y,x,z
y,-x,z
-x,-y,-z
x,y,-z
y,-x,-z
-y,x,-z
x+1/2,y+1/2,z+1/2
-x+1/2,-y+1/2,z+1/2
-y+1/2,x+1/2,z+1/2
y+1/2,-x+1/2,z+1/2
-x+1/2,-y+1/2,-z+1/2
x+1/2,y+1/2,-z+1/2
y+1/2,-x+1/2,-z+1/2
-y+1/2,x+1/2,-z+1/2
_cell_length_a 14.677(3)
_cell_length_b 14.677(3)
_cell_length_c 20.794(6)
_cell_angle_alpha 90.0000
_cell_angle_beta 90.0000
_cell_angle_gamma 90.0000
loop_
_atom_site_label
_atom_site_type_symbol
_atom_site_fract_x
_atom_site_fract_y
_atom_site_fract_z
_atom_site_U_iso_or_equiv
_atom_site_adp_type
_atom_site_occupancy

O1	O	-0.00114	0.13240	0.06281	0.00500	Uiso	1.00
O2	O	0.16994	0.16994	0.09488	0.08000	Uiso	1.00
O3	O	0.09501	0.09501	0.16972	0.08000	Uiso	1.00
C1	C	0.15328	0.15328	0.15305	0.08000	Uiso	1.00
C2	C	0.20196	0.20196	0.20069	0.08000	Uiso	1.00
C3	C	0.19690	0.17602	0.26487	0.08000	Uiso	1.00
C4	C	0.25521	0.27621	0.18326	0.08000	Uiso	1.00

```
N1    N    0.28248   0.29817   0.11946   0.10000  Uiso   0.50
C5    C    0.37977   0.32120   0.11398   0.10000  Uiso   0.50
C6    C    0.43659   0.23915   0.09581   0.10000  Uiso   0.50
C7    C    0.47678   0.19106   0.14357   0.10000  Uiso   0.50
N2    N    0.44833   0.20978   0.03229   0.10000  Uiso   0.50
C8    C    0.50100   0.13276   0.02031   0.10000  Uiso   0.50
C9    C    0.54222   0.08514   0.07106   0.10000  Uiso   0.50
C10   C    0.52814   0.11638   0.13300   0.10000  Uiso   0.50
O5    O    0.28266   0.12085   0.00000   0.08000  Uiso   0.50
O4    O    0.10203   0.27855   0.00000   0.08000  Uiso   0.50
Cl1   Cl   0.16711   0.54299   0.34181   0.12000  Uiso   1.00
O1w   O   -0.13491  -0.08739   0.55064   0.12000  Uiso   1.00
Zr1   Zr   0.11954   0.11954   0.00000   0.00500  Uiso   1.00
Zr2   Zr   0.00000   0.00000   0.11939   0.00500  Uiso   1.00
loop_
_geom_bond_atom_site_label_1
_geom_bond_atom_site_label_2
_geom_bond_distance
_geom_bond_site_symmetry_2
_ccdc_geom_bond_type
O1    Zr2    2.272   .    S
O1    Zr1    2.209   .    S
O1    Zr1    2.182   3    S
O2    C1     1.258   .    S
O2    Zr1    2.233   .    S
O3    C1     1.258   .    S
O3    Zr2    2.233   .    S
C1    C2     1.415   .    S
C2    C3     1.390   .    A
C2    C4     1.389   .    A
C4    N1     1.423   .    S
N1    C5     1.472   .    S
C5    C6     1.513   .    S
C6    C7     1.354   .    A
C6    N2     1.400   .    A
C7    C10    1.348   .    A
N2    C8     1.392   .    A
C8    C9     1.403   .    A
C9    C10    1.383   .    A
O5    Zr1    2.394   .    S
O4    Zr1    2.348   .    S
Zr1   O1     2.209   6    S
Zr1   O5     2.394   6    S
Zr1   O1     2.182   4    S
Zr1   O1     2.182   7    S
Zr1   O4     2.348   6    S
```

Zr1	O2	2.233	6	S
Zr2	O3	2.233	2	S
Zr2	O3	2.233	3	S
Zr2	O3	2.233	4	S
Zr2	O1	2.272	2	S
Zr2	O1	2.272	3	S
Zr2	O1	2.272	4	S

Though the similarity of the X-ray powder diffraction patterns of **MOR-2@$Cr_2O_7^{2-}$** and **MOR-2@CrO_4^{2-}** with that of **MOR-2** can be considered as strong evidence of their isostructurallity with the parent material, the structure solution and refinement procedure was repeated for them as well.

The patterns were indexed successfully to very similar cells, and the space group was left I4/m (Fig. S10 and S13). The first approach to structure solution was to keep the 8-connected network rigid and allow the Cr(IV) species free to move in the cell, in addition to the torsion angles related with the terephthalate substituent. All of the resulting solutions showed the Cr(IV) species in very close proximity to the Zr_6O_8 core and in some cases chromate and dichromate oxygen atoms were overlapping with the terminal oxygen atoms of the equatorial plane. The next step was to replace the terminal oxygen atom with bridging Cr(IV) species, allowing related bond lengths and angles free to move. In this way reasonable models were obtained which refined successfully (Fig. S11, S14). The crystallographic data for **MOR-2@$Cr_2O_7^{2-}$** and **MOR-2@CrO_4^{2-}** are given in pages S24-S26 and S29-S31 respectively. Fig. S12 and S15 show the packing of the crystal structures of **MOR-2@$Cr_2O_7^{2-}$** and **MOR-2@CrO_4^{2-}** respectively.

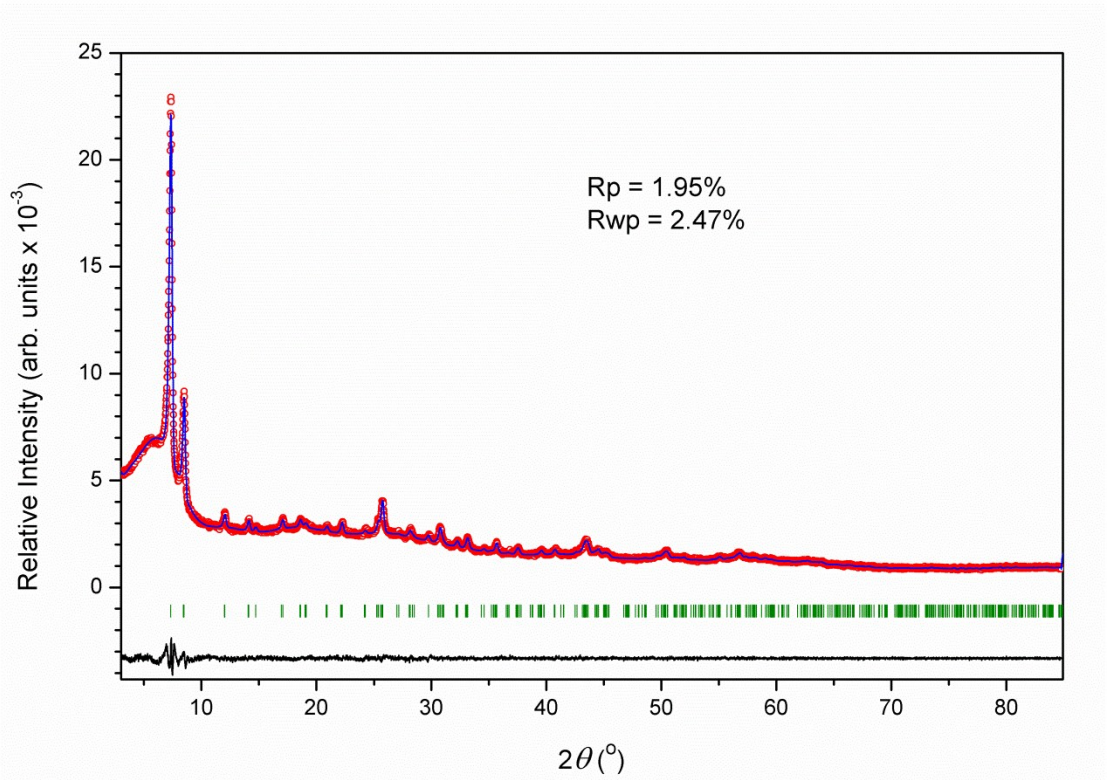

Figure S10. Structureless pattern profile refinement plot of **MOR-2@$Cr_2O_7^{2-}$** (space group: *I4/m*) (λ_{CuKa} = 1.54056). Red: experimental points; blue: calculated points; green: Bragg peaks; black: difference pattern (exp.-calc.).

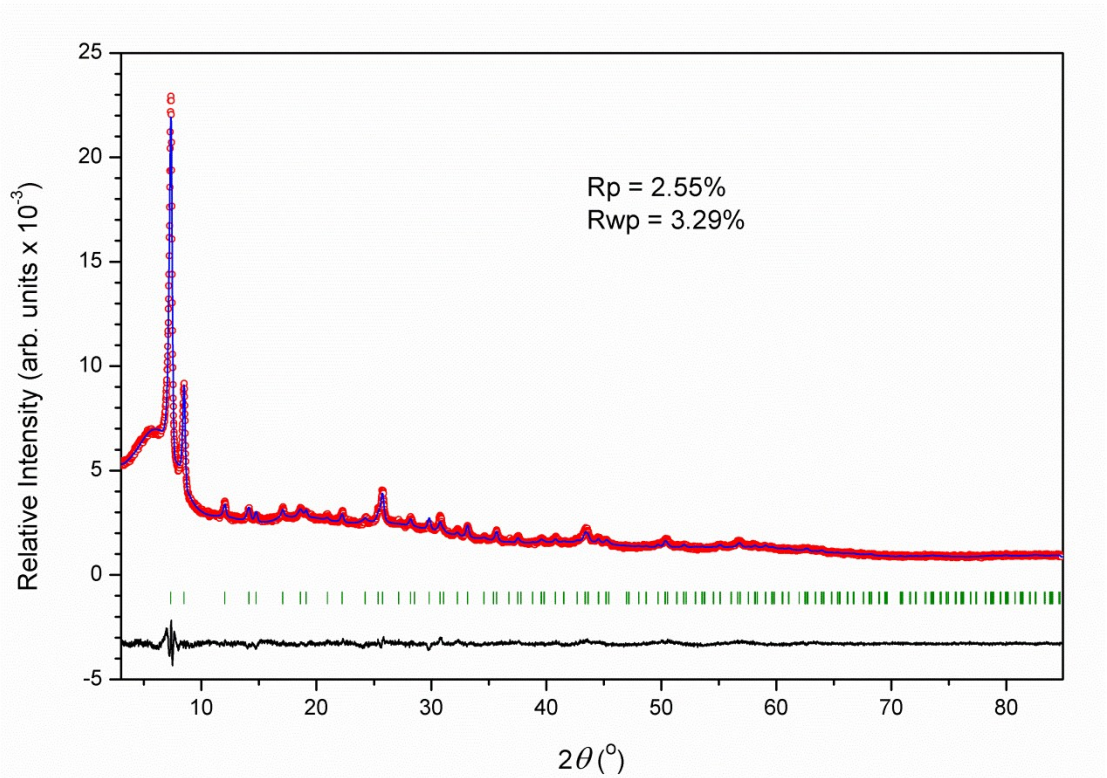

Figure S11. Rietveld plot of **MOR-2@$Cr_2O_7^{2-}$.** Red: experimental points; blue: calculated points; green: Bragg peaks; black: difference pattern (exp. – calc.).

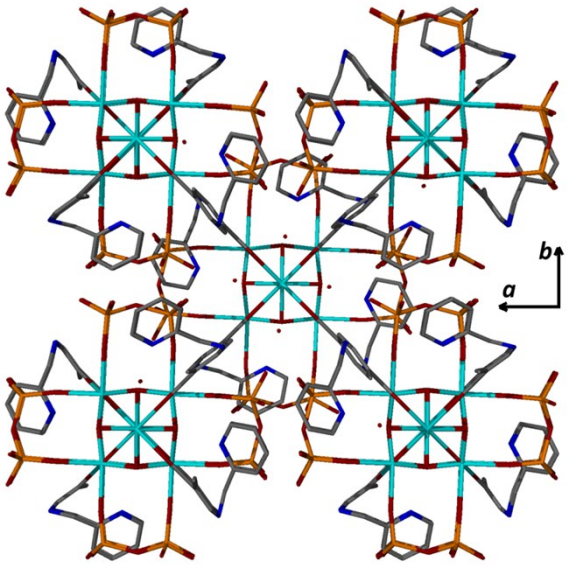

Figure S12. A packing diagram of **MOR-2@$Cr_2O_7^{2-}$** down to *c* axis. Color code: Zr, sky blue; O, red; C, grey; N, blue; Cr, orange.

data_**MOR-2@$Cr_2O_7^{2-}$**
_audit_creation_date 2017-04-03
_audit_creation_method 'Materials Studio'
_symmetry_space_group_name_H-M 'I4/M'
_symmetry_Int_Tables_number 87
_symmetry_cell_setting tetragonal
loop_
_symmetry_equiv_pos_as_xyz
x,y,z
-x,-y,z
-y,x,z
y,-x,z
-x,-y,-z
x,y,-z
y,-x,-z
-y,x,-z
x+1/2,y+1/2,z+1/2
-x+1/2,-y+1/2,z+1/2
-y+1/2,x+1/2,z+1/2
y+1/2,-x+1/2,z+1/2
-x+1/2,-y+1/2,-z+1/2
x+1/2,y+1/2,-z+1/2
y+1/2,-x+1/2,-z+1/2
-y+1/2,x+1/2,-z+1/2
_cell_length_a 14.660(2)
_cell_length_b 14.660(2)
_cell_length_c 20.709(3)
_cell_angle_alpha 90.0000
_cell_angle_beta 90.0000
_cell_angle_gamma 90.0000
loop_
_atom_site_label
_atom_site_type_symbol
_atom_site_fract_x
_atom_site_fract_y
_atom_site_fract_z
_atom_site_U_iso_or_equiv
_atom_site_adp_type
_atom_site_occupancy

O1	O	-0.00114	0.13240	0.06281	0.05000	Uiso	1.00
O2	O	0.16994	0.16994	0.09488	0.08000	Uiso	1.00
O3	O	0.09501	0.09501	0.16972	0.08000	Uiso	1.00
C1	C	0.15328	0.15328	0.15305	0.08000	Uiso	1.00
C2	C	0.20196	0.20196	0.20069	0.08000	Uiso	1.00
C3	C	0.19690	0.17602	0.26487	0.08000	Uiso	1.00
C4	C	0.25521	0.27621	0.18326	0.08000	Uiso	1.00

```
N1    N    0.28248   0.29817   0.11946   0.10000  Uiso   0.50
C5    C    0.30208   0.21760   0.07969   0.10000  Uiso   0.50
C6    C    0.33559   0.13834   0.11968   0.10000  Uiso   0.50
C7    C    0.41196   0.15049   0.15504   0.10000  Uiso   0.50
N2    N    0.29071   0.05380   0.12270   0.10000  Uiso   0.50
C10   C    0.32611  -0.01479   0.16151   0.10000  Uiso   0.50
C9    C    0.40589   0.00015   0.19703   0.10000  Uiso   0.50
C8    C    0.44741   0.08493   0.19284   0.10000  Uiso   0.50
O1W   O    0.51101   0.33714   0.21281   0.12000  Uiso   0.98
O19   O    0.43359   0.15207   0.06672   0.10000  Uiso   0.50
O17   O    0.28484   0.12515   0.00304   0.10000  Uiso   0.50
O18   O    0.44180   0.16879   0.05970   0.10000  Uiso   0.50
O20   O    0.42594  -0.00511   0.01189   0.10000  Uiso   0.50
O21   O    0.43494  -0.08629  -0.10864   0.10000  Uiso   0.50
O22   O    0.44328  -0.19078  -0.00431   0.10000  Uiso   0.50
O23   O    0.28634  -0.11246  -0.03925   0.10000  Uiso   0.50
Cr2   Cr   0.39568  -0.10238  -0.03737   0.10000  Uiso   0.50
Zr1   Zr   0.11954   0.11954   0.00000   0.05000  Uiso   1.00
Cr1   Cr   0.39442   0.11470   0.00000   0.10000  Uiso   1.00
Zr2   Zr   0.00000   0.00000   0.11939   0.05000  Uiso   1.00
loop_
_geom_bond_atom_site_label_1
_geom_bond_atom_site_label_2
_geom_bond_distance
_geom_bond_site_symmetry_2
_ccdc_geom_bond_type
O1    Zr1    2.204   .    S
O1    Zr2    2.267   .    S
O1    Zr1    2.177   3    S
O2    C1     1.253   .    S
O2    Zr1    2.225   .    S
O3    C1     1.256   .    S
O3    Zr2    2.229   .    S
C1    C2     1.411   .    S
C2    C3     1.384   .    S
C2    C4     1.387   .    S
C3    C4     1.462   13   S
C4    N1     1.417   .    S
C4    C3     1.462   13   S
N1    C5     1.468   .    S
C5    C6     1.509   .    S
C6    C7     1.350   .    S
C6    N2     1.405   .    S
C7    C8     1.344   .    S
N2    C10    1.388   .    S
C10   C9     1.399   .    S
```

C9	C8	1.387	.	S
O19	Cr1	1.593	.	S
O17	Zr1	2.426	.	S
O17	Cr1	1.615	.	S
O18	Cr1	1.625	.	S
O20	Cr2	1.809	.	S
O20	Cr1	1.833	.	S
O20	Cr2	1.584	6	S
O21	Cr2	1.602	.	S
O22	Cr2	1.623	.	S
O22	Cr2	1.706	6	S
O23	Cr2	1.610	.	S
O23	O23	1.626	6	S
O23	Cr2	2.260	6	S
Cr2	O20	1.584	6	S
Cr2	O22	1.706	6	S
Cr2	O23	2.260	6	S
Cr2	Cr2	1.548	6	S
Zr1	O2	2.225	6	S
Zr1	O1	2.204	6	S
Zr1	O17	2.426	6	S
Zr1	O1	2.177	4	S
Zr1	O1	2.177	7	S
Cr1	O19	1.593	6	S
Cr1	O17	1.615	6	S
Cr1	O18	1.625	6	S
Cr1	O20	1.833	6	S
Zr2	O1	2.267	2	S
Zr2	O1	2.267	3	S
Zr2	O1	2.267	4	S
Zr2	O3	2.229	2	S
Zr2	O3	2.229	3	S
Zr2	O3	2.229	4	S

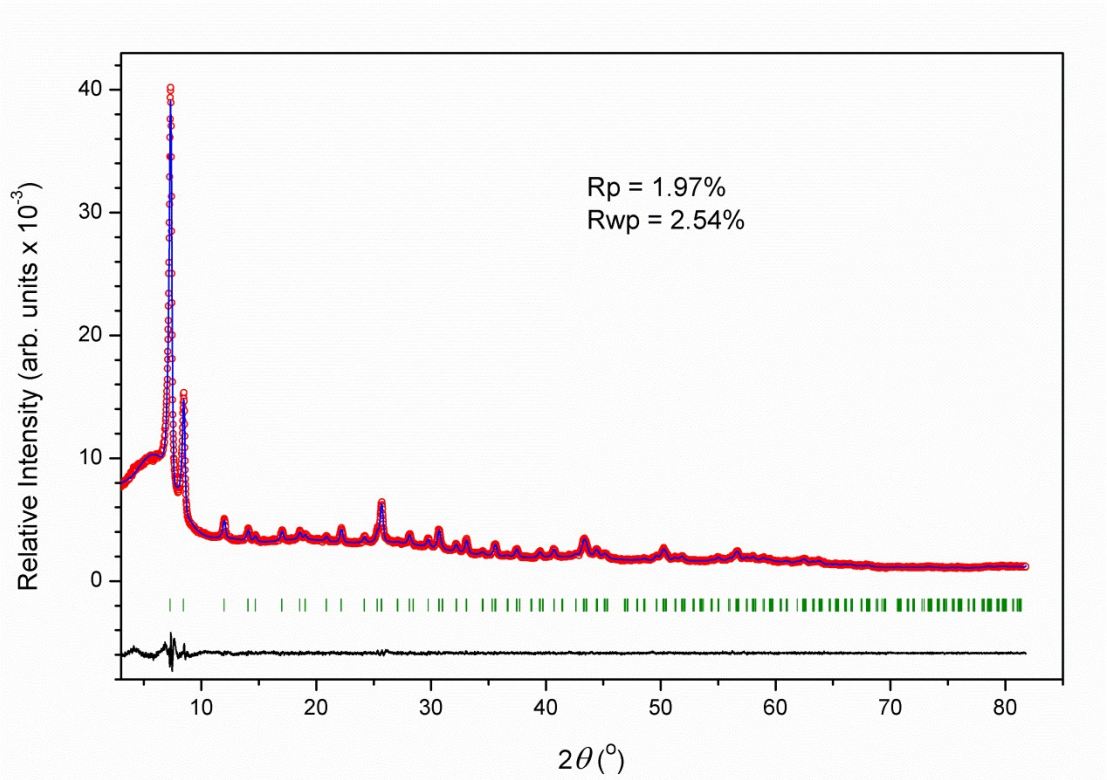

Figure S13. Structureless pattern profile refinement plot of **MOR-2@CrO_4^{2-}** (space group: I4/m) (λ_{CuKa} = 1.54056). Red: experimental points; blue: calculated points; green: Bragg peaks; black: difference pattern (exp.-calc.).

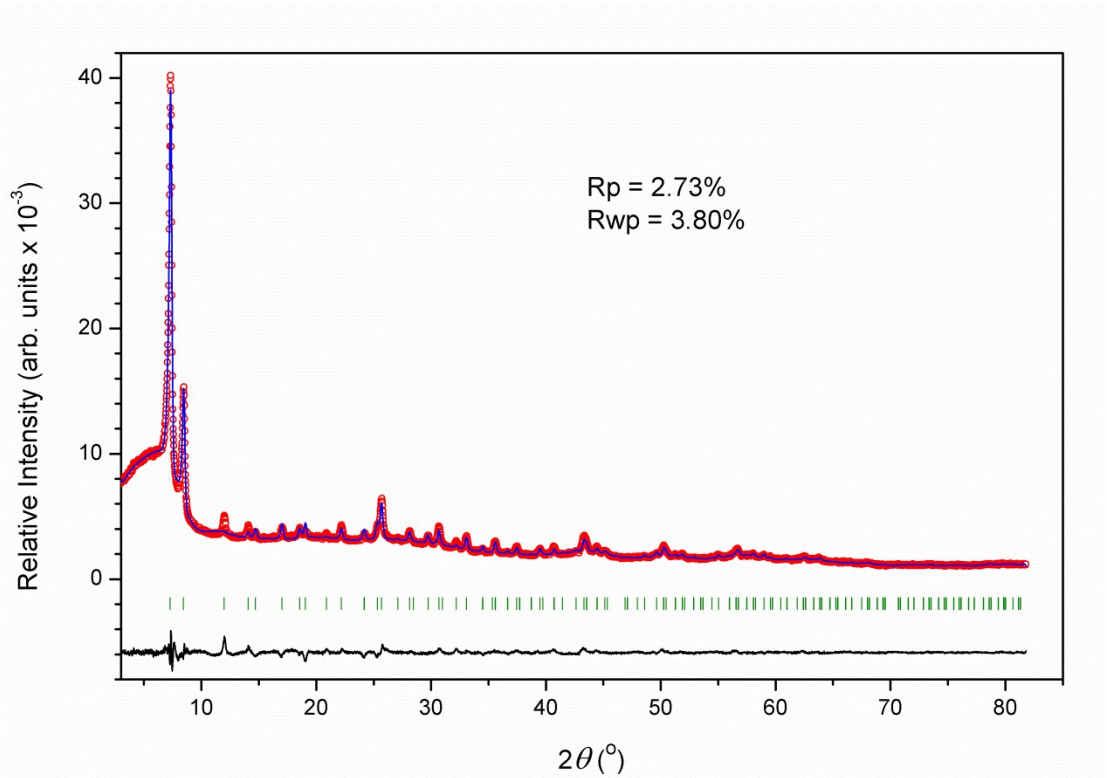

Figure S14. Rietveld plot of **MOR-2@CrO_4^{2-}.** Red: experimental points; blue: calculated points; green: Bragg peaks; black: difference pattern (exp. – calc.).

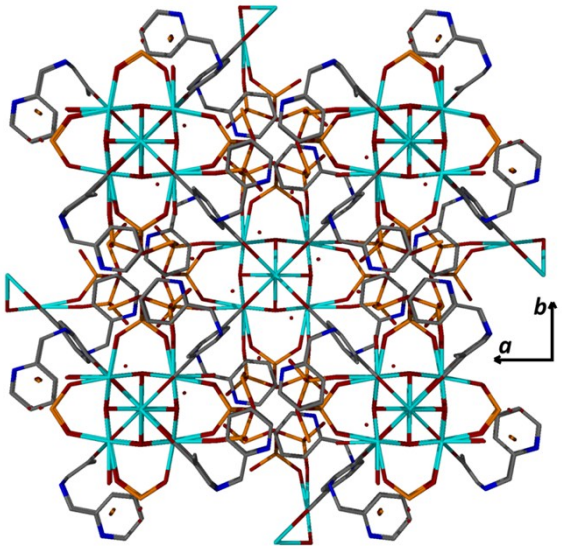

Figure S15. A packing diagram of **MOR-2@CrO_4^{2-}** down to *c* axis. Color code: Zr, sky blue; O, red; C, grey; N, blue; Cr, orange.

data_**MOR-2@CrO_4^{2-}**
_audit_creation_date 2017-04-03
_audit_creation_method 'Materials Studio'
_symmetry_space_group_name_H-M 'I4/M'
_symmetry_Int_Tables_number 87
_symmetry_cell_setting tetragonal
loop_
_symmetry_equiv_pos_as_xyz
x,y,z
-x,-y,z
-y,x,z
y,-x,z
-x,-y,-z
x,y,-z
y,-x,-z
-y,x,-z
x+1/2,y+1/2,z+1/2
-x+1/2,-y+1/2,z+1/2
-y+1/2,x+1/2,z+1/2
y+1/2,-x+1/2,z+1/2
-x+1/2,-y+1/2,-z+1/2
x+1/2,y+1/2,-z+1/2
y+1/2,-x+1/2,-z+1/2
-y+1/2,x+1/2,-z+1/2
_cell_length_a 14.671(2)
_cell_length_b 14.671(2)
_cell_length_c 20.730(4)
_cell_angle_alpha 90.0000
_cell_angle_beta 90.0000
_cell_angle_gamma 90.0000
loop_
_atom_site_label
_atom_site_type_symbol
_atom_site_fract_x
_atom_site_fract_y
_atom_site_fract_z
_atom_site_U_iso_or_equiv
_atom_site_adp_type
_atom_site_occupancy

O1	O	-0.00114	0.13240	0.06281	0.05000	Uiso	1.00
O4	O	0.16994	0.16994	0.09488	0.08000	Uiso	1.00
O3	O	0.09501	0.09501	0.16972	0.08000	Uiso	1.00
C1	C	0.15328	0.15328	0.15305	0.08000	Uiso	1.00
C2	C	0.20196	0.20196	0.20069	0.08000	Uiso	1.00
C3	C	0.19690	0.17602	0.26487	0.08000	Uiso	1.00
C4	C	0.25521	0.27621	0.18326	0.08000	Uiso	1.00

```
N1    N    0.28248   0.29817   0.11946   0.10000  Uiso   0.50
C9    C    0.37195   0.26046   0.10206   0.10000  Uiso   0.50
C10   C    0.38953   0.16984   0.13440   0.10000  Uiso   0.50
C11   C    0.32063   0.10856   0.13652   0.10000  Uiso   0.50
N2    N    0.47380   0.14581   0.16119   0.10000  Uiso   0.50
C14   C    0.48385   0.06033   0.18928   0.10000  Uiso   0.50
C13   C    0.41059  -0.00106   0.19104   0.10000  Uiso   0.50
C12   C    0.32892   0.02549   0.16356   0.10000  Uiso   0.50
Cr1A  Cr   0.49785   0.83245   0.48316   0.10000  Uiso   0.25
O2A   O    0.49512   0.87439   0.41052   0.10000  Uiso   0.25
O4A   O    0.40931   0.76761   0.49494   0.10000  Uiso   0.25
O1A   O    0.59033   0.77239   0.49238   0.10000  Uiso   0.25
O3A   O    0.49612   0.91553   0.53518   0.10000  Uiso   0.25
O5B   O    0.62544   0.77011   0.48343   0.10000  Uiso   0.25
O7B   O    0.68957   0.93843   0.46680   0.10000  Uiso   0.25
O6B   O    0.63224   0.88479   0.58192   0.10000  Uiso   0.25
O4B   O    0.50503   0.91971   0.48310   0.10000  Uiso   0.25
O3B   O    0.38745   0.89013   0.58646   0.10000  Uiso   0.25
O2B   O    0.32004   0.94565   0.47427   0.10000  Uiso   0.25
O1B   O    0.38126   0.77539   0.48845   0.10000  Uiso   0.25
Cr2B  Cr   0.61711   0.87555   0.50484   0.10000  Uiso   0.25
Cr1B  Cr   0.39405   0.88030   0.50930   0.10000  Uiso   0.25
 O1W  O   -0.16010   1.05954  -0.57095   0.12000  Uiso   0.73
Zr1   Zr   0.11954   0.11954   0.00000   0.05000  Uiso   1.00
Zr2   Zr   0.00000   0.00000   0.11939   0.05000  Uiso   1.00
loop_
_geom_bond_atom_site_label_1
_geom_bond_atom_site_label_2
_geom_bond_distance
_geom_bond_site_symmetry_2
_ccdc_geom_bond_type
O1    Zr1    2.206   .    S
O1    Zr2    2.269   .    S
O1    Zr1    2.179   3    S
O4    C1     1.254   .    S
O4    Zr1    2.228   .    S
O3    C1     1.257   .    S
O3    Zr2    2.230   .    S
C1    C2     1.413   .    S
C2    C3     1.386   .    S
C2    C4     1.388   .    S
C3    C4     1.463   13   S
C4    N1     1.419   .    S
C4    C3     1.463   13   S
N1    C9     1.469   .    S
C9    C10    1.511   .    S
```

C10	C11	1.353	.	S
C10	N2	1.401	.	S
C11	C12	1.347	.	S
N2	C14	1.391	.	S
C14	C13	1.403	.	S
C13	C12	1.383	.	S
Cr1A	O2A	1.627	.	S
Cr1A	O4A	1.628	.	S
Cr1A	O1A	1.629	.	S
Cr1A	O3A	1.628	.	S
O5B	Cr2B	1.614	.	S
O7B	Cr2B	1.613	.	S
O6B	Cr2B	1.619	.	S
O4B	Cr2B	1.824	.	S
O4B	Cr1B	1.811	.	S
O3B	Cr1B	1.609	.	S
O2B	Cr1B	1.620	.	S
O1B	Cr1B	1.610	.	S
Zr1	O4	2.228	6	S
Zr1	O1	2.206	6	S
Zr1	O1	2.179	4	S
Zr1	O1	2.179	7	S
Zr2	O1	2.269	2	S
Zr2	O1	2.269	3	S
Zr2	O1	2.269	4	S
Zr2	O3	2.230	2	S
Zr2	O3	2.230	3	S
Zr2	O3	2.230	4	S

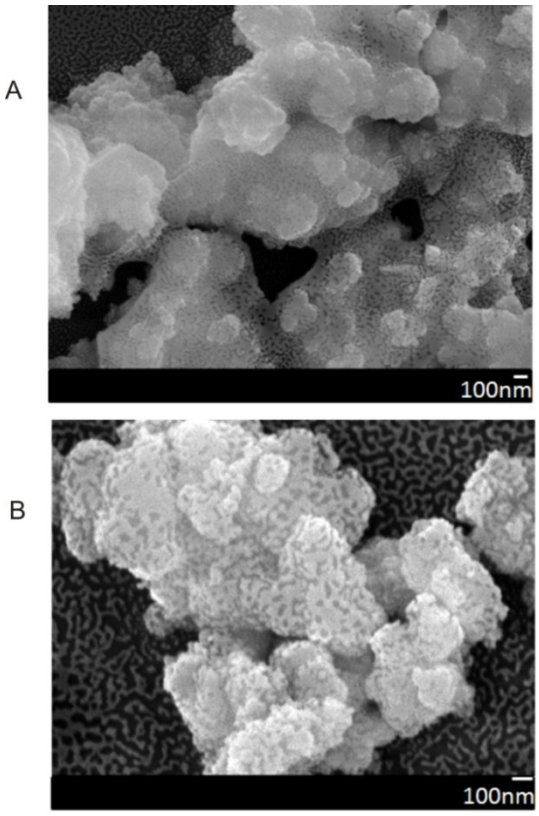

Figure S16. FE-SEM images of A. **MOR-2** and B. **MOR-2-HA.**

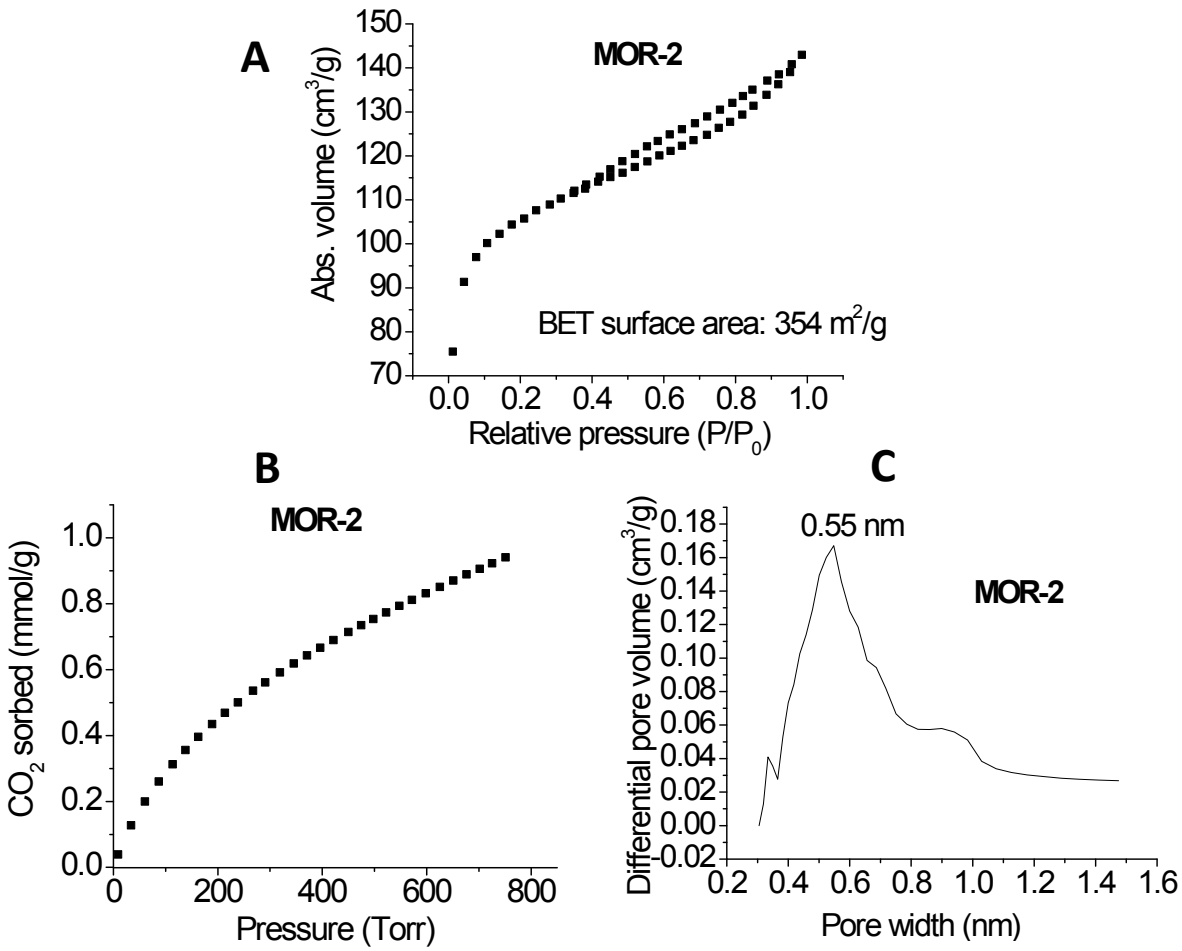

Figure S17. A) Nitrogen sorption isotherm at 77 K,B) CO_2 adsorption isotherm at 273 K and C) the resultant DFT micropore size distribution (assuming slit-type pores) for **MOR-2**. The DFT analysis of the adsorption data indicates a pore size of ~ 0.55 nm.

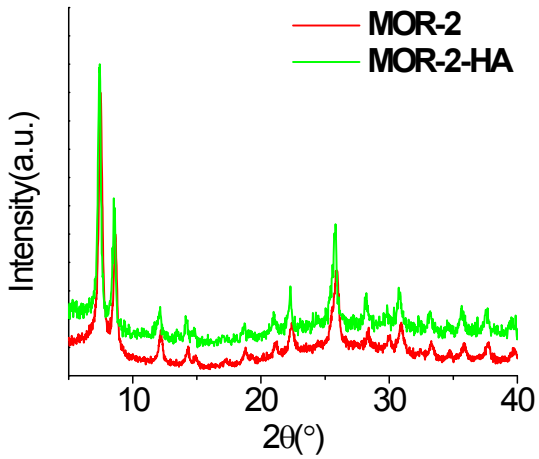

Figure S18. PXRD pattern of **MOR-2-HA** vs. that of **MOR-2**.

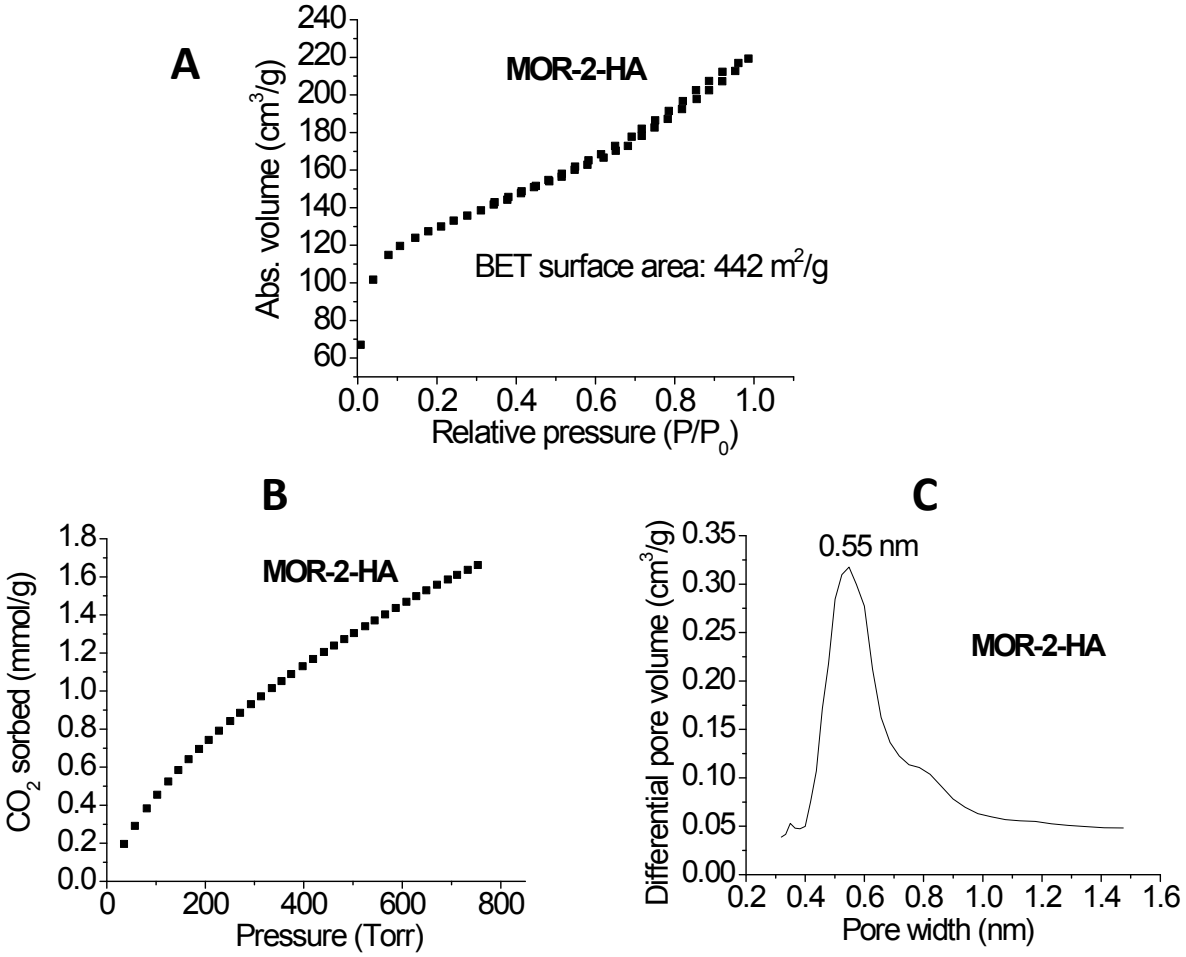

Figure S19. A) Nitrogen sorption isotherm at 77 K,B) CO_2 adsorption isotherm at 273 K and C) the resultant DFT micropore size distribution (assuming slit-type pores)for **MOR-2-HA**. The DFT analysis of the adsorption data indicates a pore size of ~ 0.55 nm.

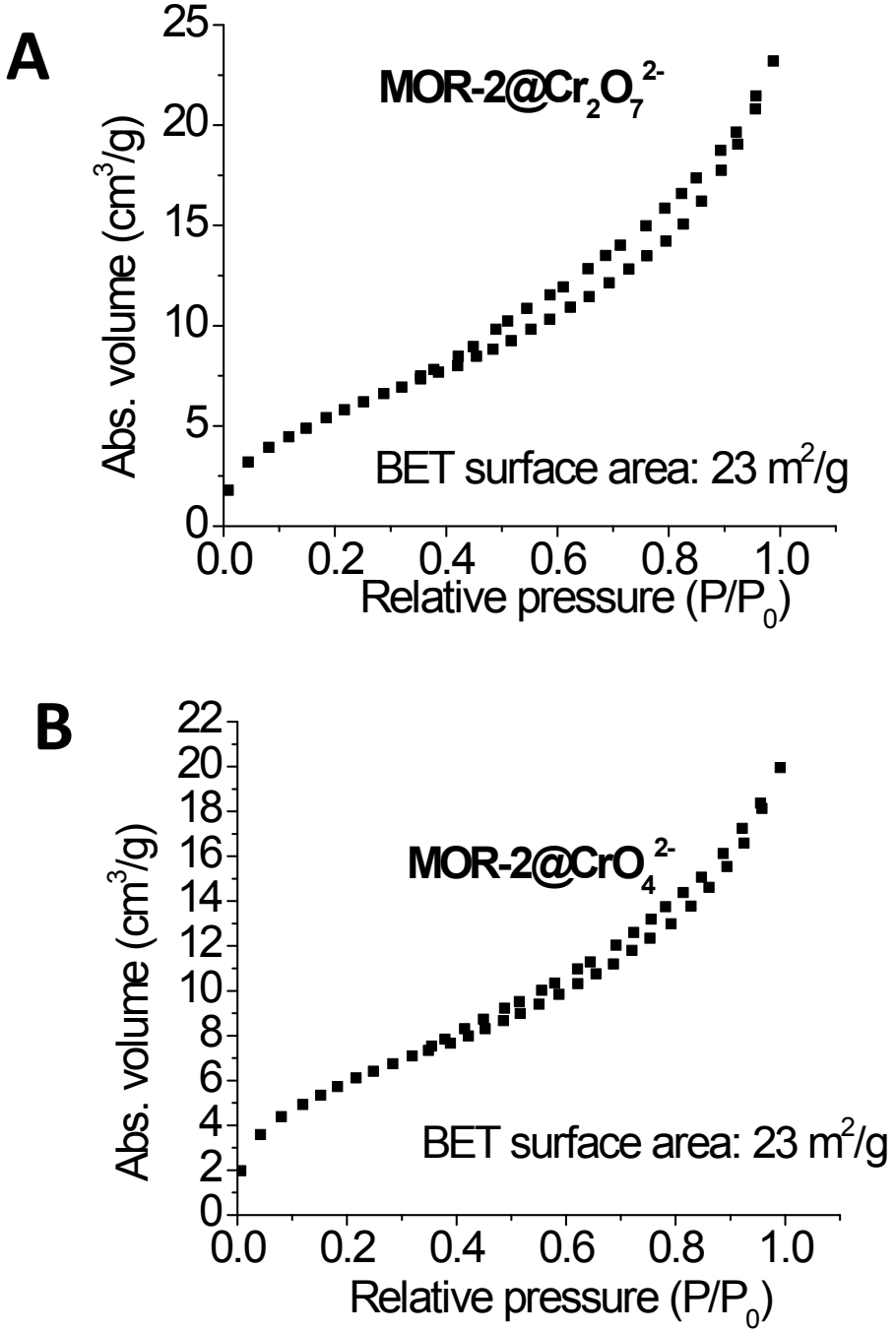

Figure S20. Nitrogen sorption isotherms at 77 K for A) **MOR-2@$Cr_2O_7^{2-}$** and B)**MOR-2@CrO_4^{2-}**.

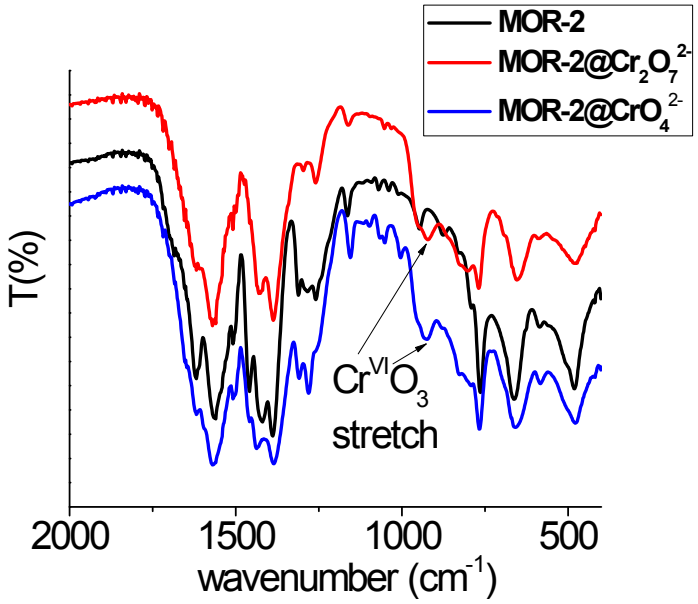

Figure S21. IR spectra of **MOR-2** and **MOR@Cr(VI)** materials.

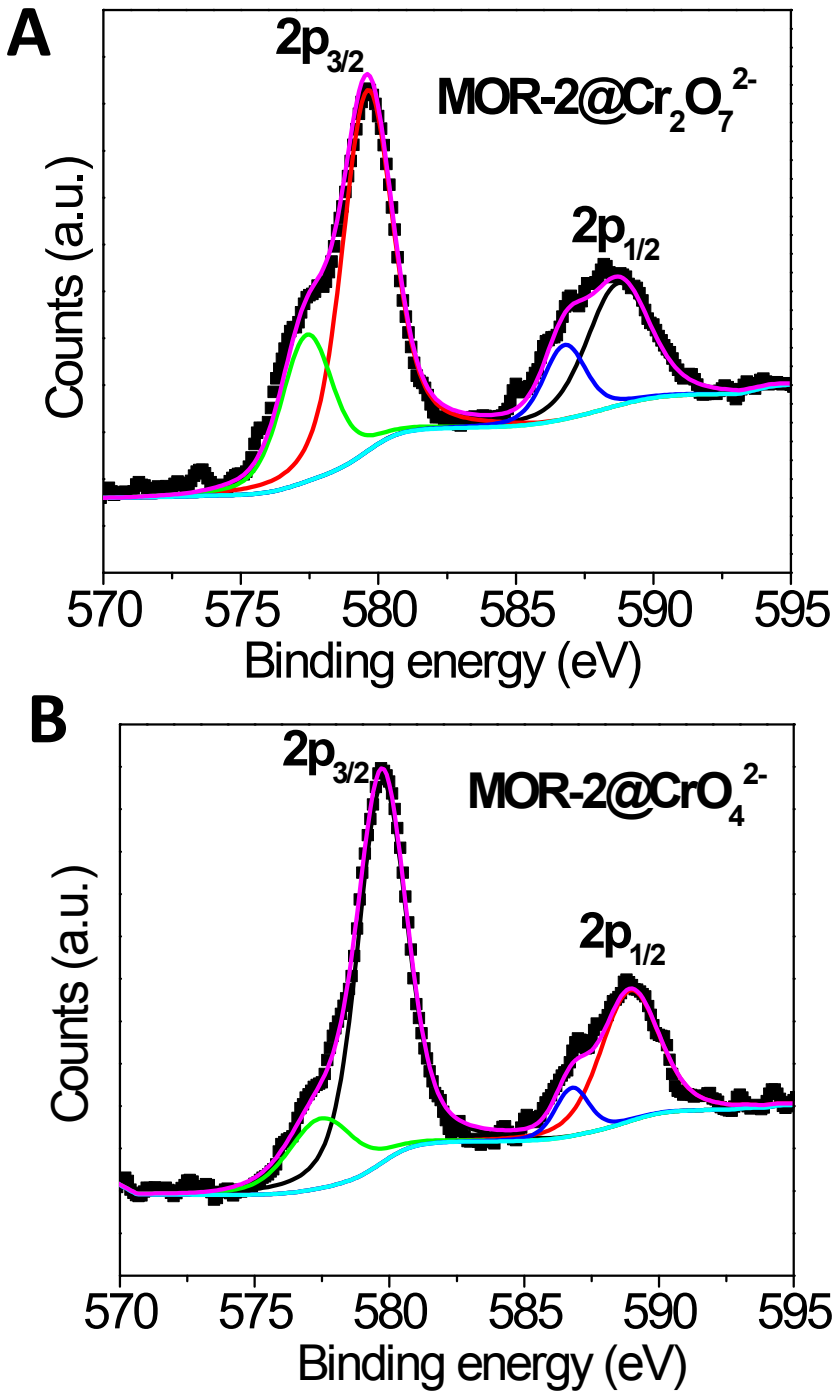

Figure S22. High resolution $Cr2p_{1/2}$ and $Cr2p_{3/2}$ core-level photoelectron spectra of **MOR-2@$Cr_2O_7^{2-}$ (A) and MOR-2@CrO_4^{2-} (B)** as well as their de-convolution into two components. The main $Cr2p_{1/2}$/$Cr2p_{3/2}$peak components appear at 588.7/579.6 and 588.9/579.7 for **MOR-**

2@$Cr_2O_7^{2-}$ and MOR-2@CrO_4^{2-}respectively. These binding energies are consistent with Cr(VI).[6]The minor signals with binding energy at 586.8 and 577.4 eV, present for both **MOR-2@$Cr_2O_7^{2-}$ and MOR-2@CrO_4^{2-},** are due to Cr(III) traces produced from the reduction effects under X-ray irradiation.[11]

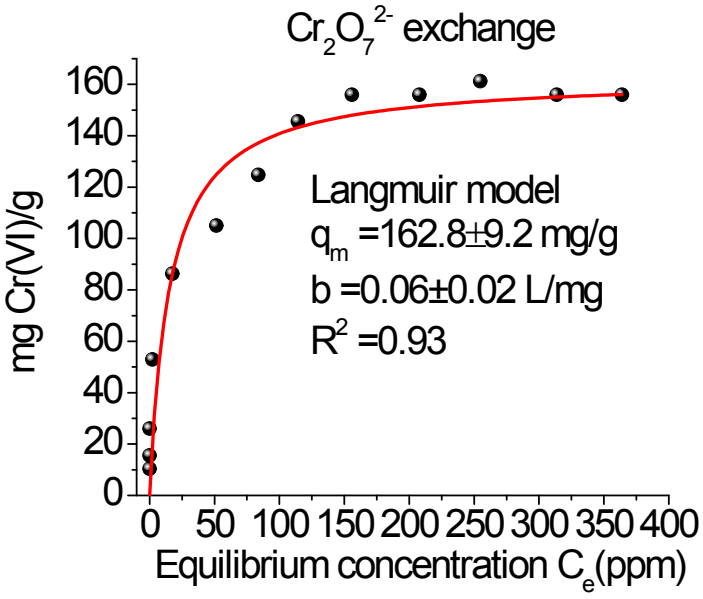

Figure S23. Isotherm dichromate ion exchange data for **MOR-2-HA**. The red line represents the fitting of the data with the Langmuir model.

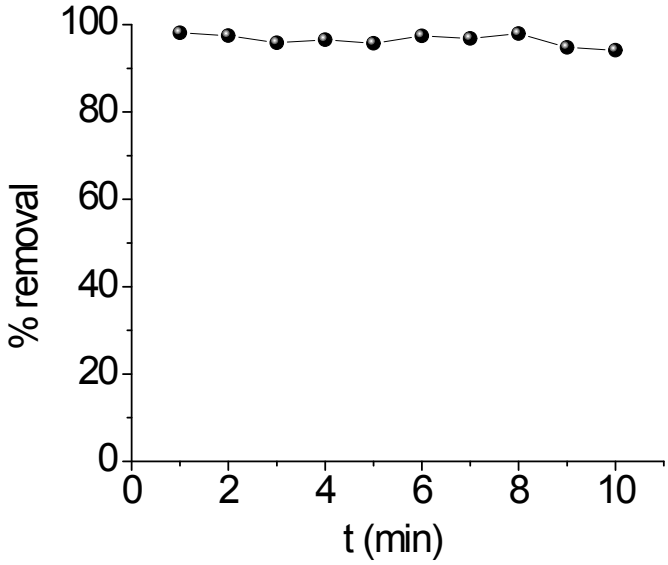

Figure S24. The kinetics of dichromate ion exchange for **MOR-2-HA** (initial dichromate concentration = 21.6 ppm, pH~3).

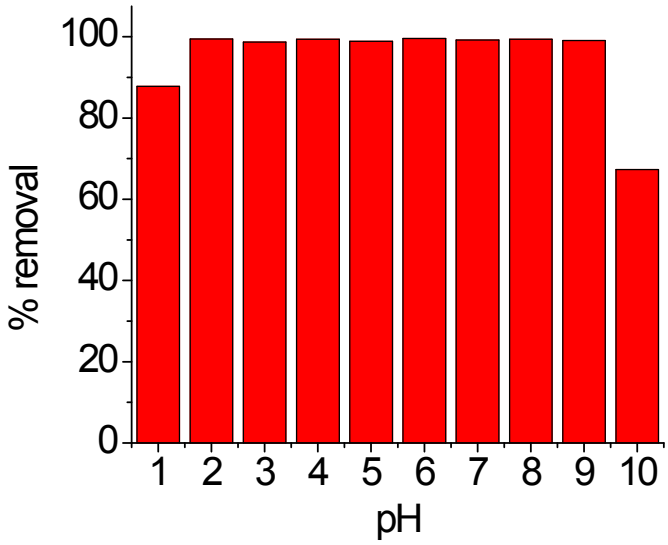

Figure S25. Total Cr removal (%) by **MOR-2** vs. pH (initial total Cr concentration = 10.4 ppm).

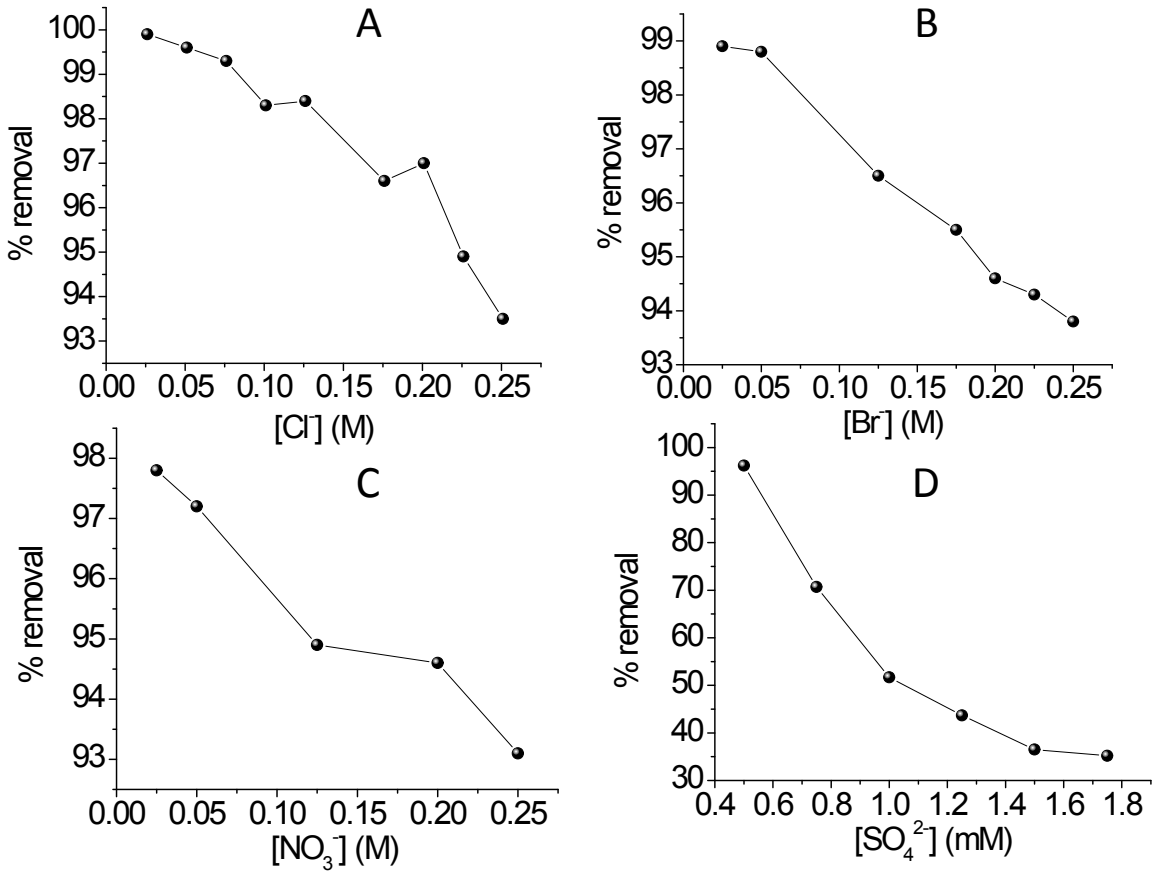

Figure S26. Selectivity ion exchange data, presented as% dichromate removal vs. A) Cl^-, B) Br^-, C) NO_3^- and D) SO_4^{2-} concentrations. The initial dichromate concentration was 0.25 mM (pH~3).

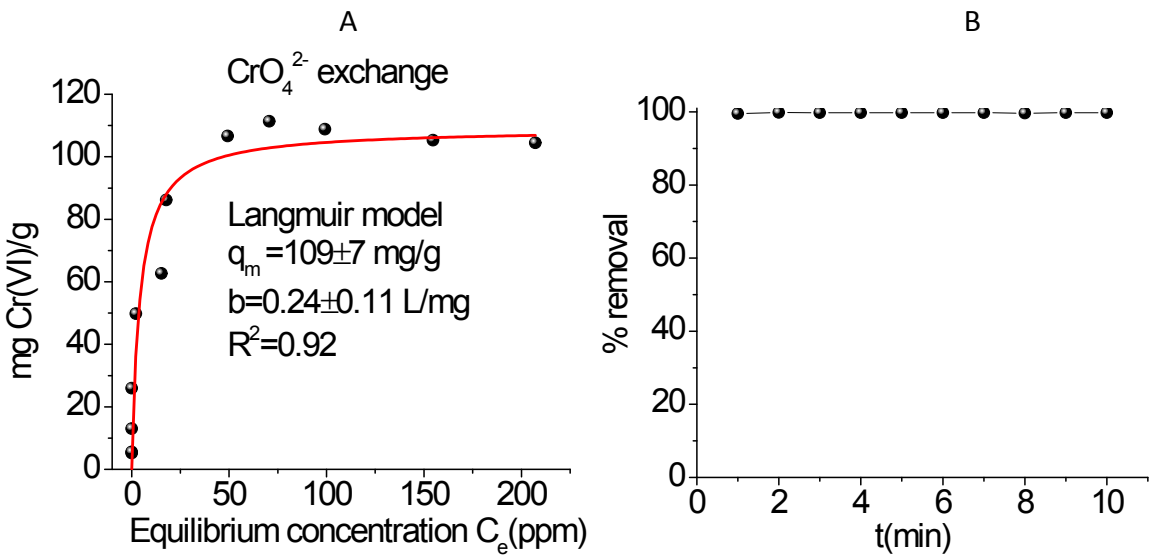

Figure S27. A. Isotherm CrO_4^{2-} exchange data and B. Kinetics of CrO_4^{2-} exchange data (initial chromate concentration =11.6 ppm, pH~7) for **MOR-2-HA**.

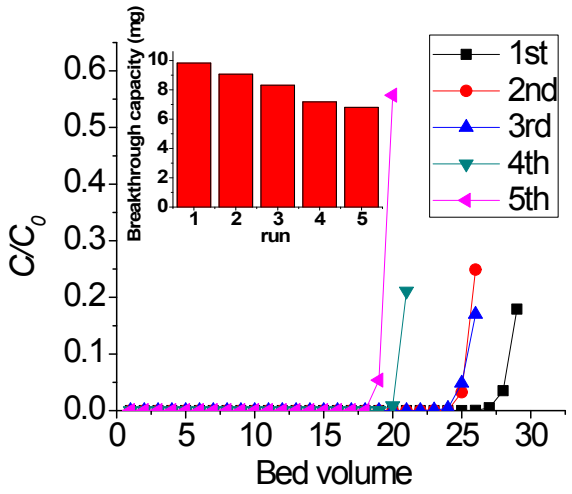

Figure S28. Breakthrough curves for five column ion exchange runs (C= $Cr_2O_7^{2-}$ concentration of the effluent, C_0 = initial $Cr_2O_7^{2-}$ concentration = 108 ppm, pH~ 3, flow rate ~ 1 mL/min, one bed volume =3.5 mL, stationary phase **MOR-2-HA**/sand =0.1 g:5 g). The lines are only a guide for the eye. Inset: Breakthrough capacities obtained from the five column ion exchange runs.

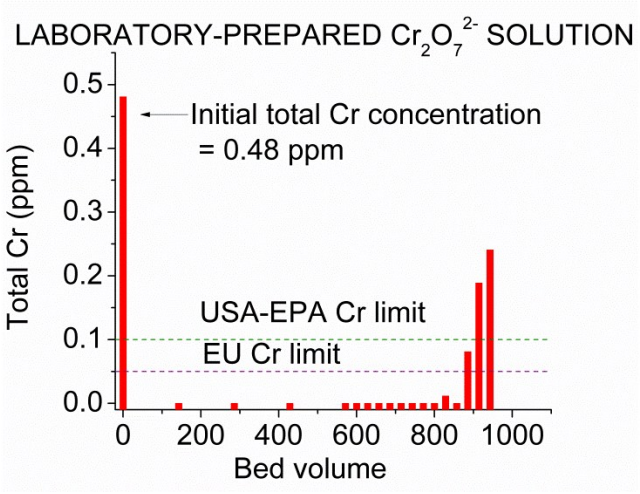

Figure S29. Total Cr content (ppm) vs. bed volume (1 bed vole = 3.5 mL) of a dichromate aqueous solution (initial total concentration = 0.48 ppm, pH~ 3), after passing it through the **MOR-2-HA**/sand column (flow rate ~ 1.75 mL/min, stationary phase **MOR-2-HA**/sand =0.05 g:5 g).

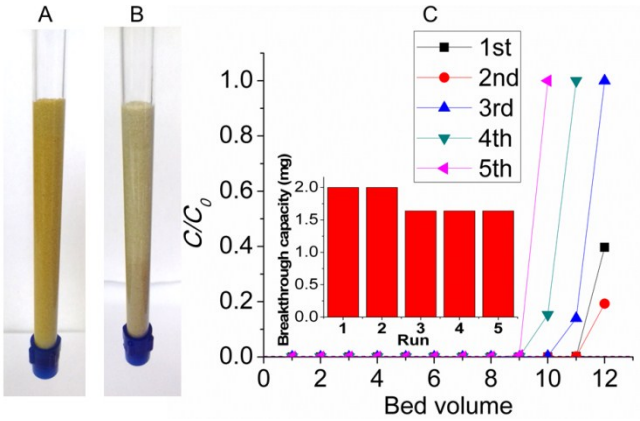

Figure S30. A. CrO_4^{2-}-loaded column B. Column after the regeneration process (it looks identical with the pristine one). C. Breakthrough curves for five column ion exchange runs (C= CrO_4^{2-} concentration of the effluent, C_0 = initial CrO_4^{2-} concentration = 52 ppm, pH~ 7, flow rate ~ 1.0 mL/min, one bed volume =3.5 mL, stationary phase MOR-2-HA/sand =0.1 g:5 g). The lines are only a guide for the eye. Inset: Breakthrough capacities obtained from the five column ion exchange runs.

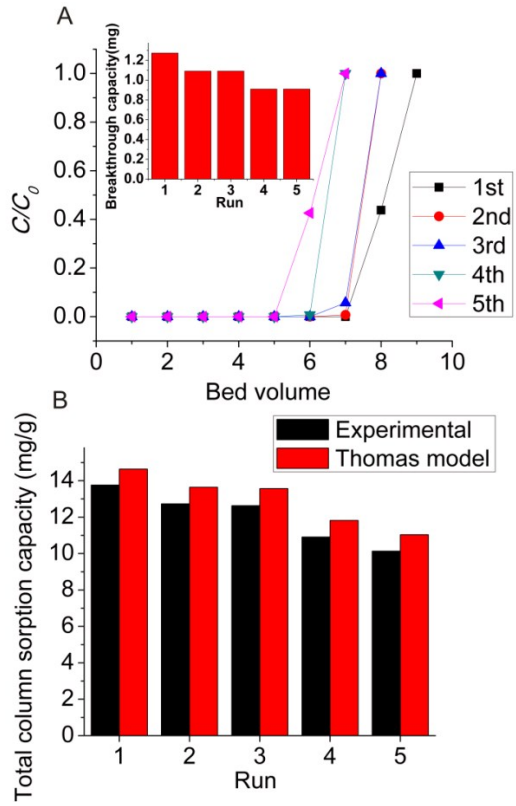

Figure S31. A. Breakthrough curves for five column ion exchange runs with the chrome plating solution B (C= CrO_4^{2-} concentration of the effluent, C_0 = initial CrO_4^{2-} concentration = 52 ppm, pH~ 8, flow rate ~ 1.0 mL/min, one bed volume =3.5 mL, stationary phase **MOR-2-HA**/sand =0.1 g:5 g). The lines are only a guide for the eye. Inset: Breakthrough capacities obtained from the five column ion exchange runs. B. The predicted (by the Thomas model) and experimentally found total column sorption capacities.

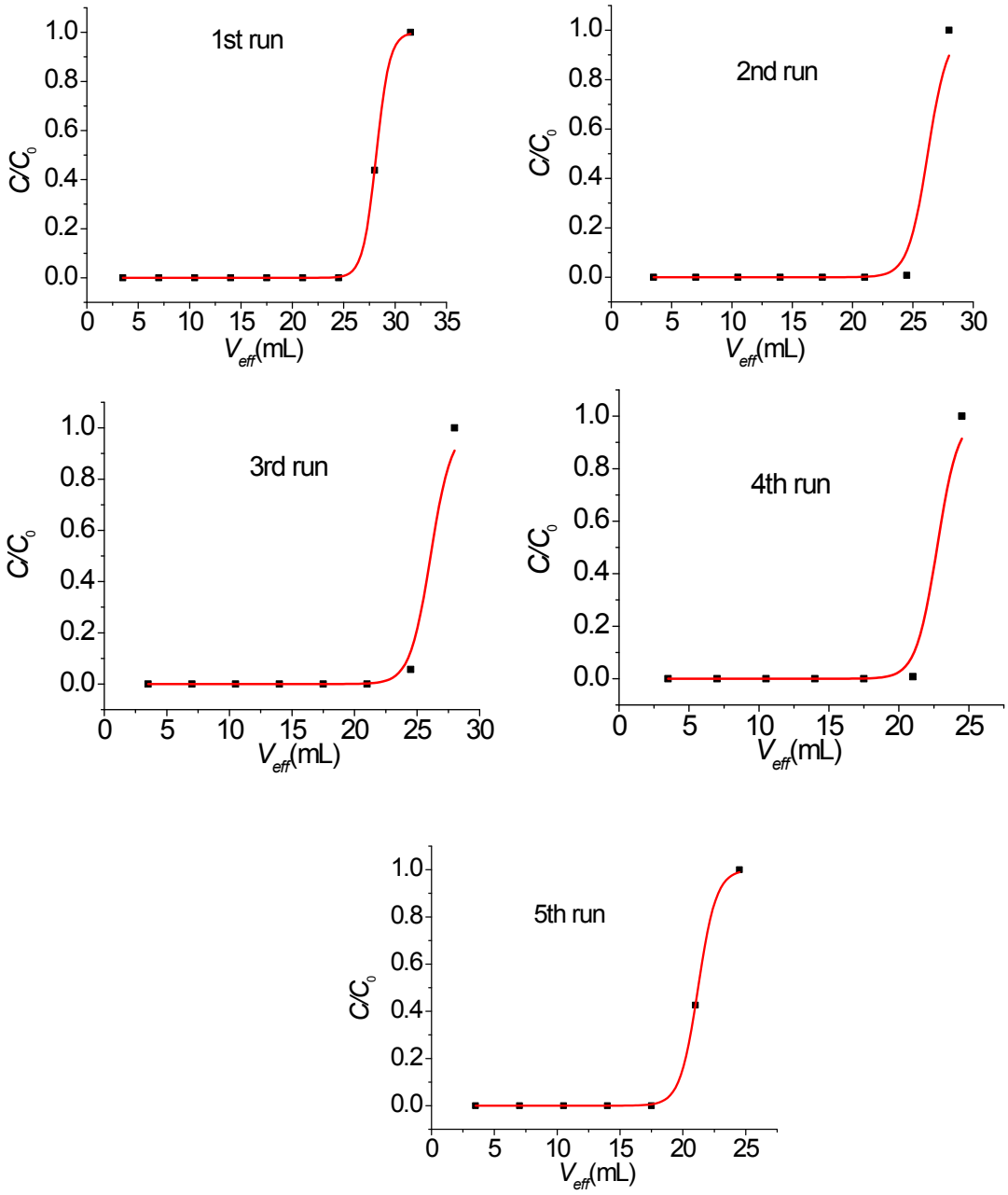

Figure S32. Fitting of the breakthrough curves (red line) for the column soprtion experiments with the chrome plating wastewater sample B.The data are fitted with an equation (Thomas model) of the type $y = \frac{1}{1+\exp(A - Bx)}$, where A $= \frac{k_{Th} q_{\max} m}{Q}$, B$= \frac{k_{Th} C_0}{Q}$.

The results of the fitting are shown in Table S1.

Table S1. Fitting of the column sorption data and the experimentally found q_{max} values.

Run	Fitting results			Thomas model parameters		Exp. found q_{max}(mg/g)
	A	B	R^2	k_{Th} (L mg^{-1} min^{-1})	q_{max}(mg/g)	
1	43.155	1.533	0.999	0.029481	14.64	13.76
2	32.209	1.228	0.973	0.023615	13.64	12.73
3	31.645	1.213	0.983	0.023327	13.57	12.63
4	30.368	1.336	0.980	0.025692	11.82	10.91
5	29.324	1.382	0.999	0.026577	11.03	10.13

Computational Details

Geometry optimizations, without symmetry constrains, were performed using the BP86 GGA functional[12,13] in combination with the 6-31G(d,p) basis set for all elements. All calculations were performed for aqueous solutions of the interacting species using the Polarizable Continuum Model (PCM) for solvation as implemented in the Gaussian 09 program suite.[14]The computational protocol used is denoted as BP86/6-31G(d,p)/PCM. All stationary points were verified as minima (number of imaginary frequencies NImag=0).The results are shown in Table S2.

Table S2. Thermodynamics (ΔH in kcal/mol) of possible reactions involved in the oxido-Cr(VI) anion exchange processes with **MOR-2** calculated at the BP86/6-31G(d,p) level of theory.

Reaction	ΔH (kcal/mol)
$[PhNH_2CH_2Py]^+ + H^+ \rightarrow [PhNH_2CH_2PyH]^{2+}$	-157.5
$[PhNHCH_2PyH]^+ + H^+ \rightarrow [PhNH_2CH_2PyH]^{2+}$	-151.7
$CrO_4^{2-} + H^+ \rightarrow HCrO_4^-$	-203.0
$Cr_2O_7^{2-} + H^+ \rightarrow HCr_2O_7^-$	-164.5
$[PhNH_2CH_2PyH]^{2+} + CrO_4^{2-} \rightarrow [PhNH_2CH_2Py]^+ + HCrO_4^-$	-45.1
$[PhNH_2CH_2PyH]^{2+} + CrO_4^{2-} \rightarrow [PhNHCH_2PyH]^+ + HCrO_4$	-51.3

$[PhNH_2CH_2PyH]^{2+} + Cr_2O_7^{2-} \rightarrow [PhNH_2CH_2Py]^{+} + HCr_2O_7^{-}$	-7.1
$[PhNH_2CH_2PyH]^{2+} + Cr_2O_7^{2-} \rightarrow [PhNH_2CH_2PyH]^{+} + HCr_2O_7^{-}$	-12.8
$[PhNH_2CH_2PyH]^{2+} + CrO_4^{2-} \rightarrow [PhNH_2CH_2PyH(CrO_4^{2-})]$	-59.6
$[PhNH_2CH_2PyH]^{2+} + CrO_4^{2-} \rightarrow [PhNH_2(CrO_4^{2-})CH_2PyH]$	-61.3
$[PhNH_2CH_2Py]^{+} + HOCrO_3^{-} \rightarrow [PhNH_2CH_2Py(HOCrO_3^{-})]$	-11.6
$[PhNH_2CH_2PyH]^{2+} + HOCrO_3^{-} \rightarrow [PhNH_2CH_2PyH(HOCrO_3^{-})]^{+}$	-23.9
$[PhNH_2CH_2PyH]^{2+} + Cr_2O_7^{2-} \rightarrow [PhNH_2CH_2PyH(Cr_2O_7^{2-})]$	-37.3

Calculations were also performed using the dispersion–corrected wB97XD density functional[15] in combination with the Def2-TZVPPD basis set for all elements.[16] However, most of the calculations using the wB97XD/Def2-TZVPPD/PCM computational protocol failed, due to SCF convergence problems. In the cases where calculations performed successfully the results obtained (Table S3) are almost identical to those obtained using the BP86/6-31G(d,p)/PCM protocol.

Table S3. Thermodynamics (*ΔH* in kcal/mol) of possible reactions involved in the oxido-Cr(VI) anion exchange processes with **MOR-2** calculated at the wB97XD/Def2-TZVPP level of theory.

Reaction	*ΔH* (kcal/mol)
$[PhNH_2CH_2Py]^{+} + H^{+} \rightarrow [PhNH_2CH_2PyH]^{2+}$	-160.4 (-157.5)[a]
$[PhNHCH_2PyH]^{+} + H^{+} \rightarrow [PhNH_2CH_2PyH]^{2+}$	-152.0 (-151.7)
$CrO_4^{2-} + H^{+} \rightarrow HCrO_4^{-}$	-194.6 (-203.0)
$Cr_2O_7^{2-} + H^{+} \rightarrow HCr_2O_7^{-}$	-164.2 (-164.5)
$[PhNH_2CH_2PyH]^{2+} + CrO_4^{2-} \rightarrow [PhNH_2CH_2Py]^{+} + HCrO_4^{-}$	failed
$[PhNH_2CH_2PyH]^{2+} + CrO_4^{2-} \rightarrow [PhNHCH_2PyH]^{+} + HCrO_4$	failed
$[PhNH_2CH_2PyH]^{2+} + Cr_2O_7^{2-} \rightarrow [PhNH_2CH_2Py]^{+} + HCr_2O_7^{-}$	failed
$[PhNH_2CH_2PyH]^{2+} + Cr_2O_7^{2-} \rightarrow [PhNHCH_2PyH]^{+} + HCr_2O_7^{-}$	failed
$[PhNH_2CH_2PyH]^{2+} + CrO_4^{2-} \rightarrow [PhNHCH_2PyH(CrO_4^{2-})]$	failed
$[PhNH_2CH_2PyH]^{2+} + CrO_4^{2-} \rightarrow [PhNH_2(CrO_4^{2-})CH_2PyH]$	failed
$[PhNH_2CH_2Py]^{+} + HOCrO_3^{-} \rightarrow [PhNHCH_2Py(HOCrO_3^{-})]$	failed

$[PhNH_2CH_2PyH]^{2+} + HOCrO_3^- \rightarrow [PhNHCH_2PyH(HOCrO_3^-)]^+$	failed
$[PhNH_2CH_2PyH]^{2+} + Cr_2O_7^{2-} \rightarrow [PhNH_2CH_2PyH(Cr_2O_7^{2-})]$	failed

[a] Figures in parentheses are the results obtained by the BP86/6-31G(d,p)/PCM protocol.

Discussion of the theoretical calculations

In aqueous solution hexavalent chromium exists as oxido- forms in a variety of species depending on pH and Cr(VI) concentration (see reference 1, main text) . For the oxo species of hexavalent chromium three main pH regions may be distinguished:

(1) H_2CrO_4 (pH < 0),

(2) $HCrO_4^-$and $Cr_2O_7^{2-}$ (pH 2–6),

(3) CrO_4^{2-} (pH > 6).

Which entity will dominate in a particular environment depends upon the specific conditions, for example, pH, E_h (redox potential), total concentration of chromium, and the overall aqueous chemistry.

Therefore, we explored the possible interaction modes of **MOR-2@CrO_4^{2-}**, **MOR-2@$HCrO_4^-$** and **MOR-2@$Cr_2O_7^{2-}$** and the thermodynamics of possible reactions involved in the oxido-Cr(VI) anion exchange processes by means of DFT computational protocols (computational details are given above). The enthalpy changes (ΔH in kcal/mol) of all possible reactions calculated at the BP86/6-31G(d,p) level of theory are given in Table S2. Comparable results are obtained employing the wB97XD/Def2-TZVPP DFT method (see above).

The proton affinities of pyridine and methylamine moieties of the $PhNHCH_2Py$ ligand used as a model of the PATP ligand predicted to be -157.5 and -151.7 kcal/mol respectively at the BP86/6-31G(d,p) level of theory indicate the slightly more basic character of pyridine than methylamine moieties. On the other hand, the proton affinities of CrO_4^{2-} and $Cr_2O_7^{2-}$ are predicted to be -203.0 and -164.5 kcal/mol respectively. The detachment of the proton either from the pyridinium or methylammonium moieties of the $[PhNH_2CH_2PyH]^{2+}$ ligand by the CrO_4^{2-} dianions according to the reactions (eq. 1,2):

$[PhNH_2CH_2PyH]^{2+} + CrO_4^{2-} \rightarrow [PhNH_2CH_2Py]^{+} + HCrO_4^{-}$ (1)

$[PhNH_2CH_2PyH]^{2+} + CrO_4^{2-} \rightarrow [PhNHCH_2PyH]^{+} + HCrO_4^{-}$(2)

are slightly less exothermic (-45.1 kcal/mol) for the proton detachment process from pyridinium than methylammonium moieties (-51.3 kcal/mol). The deprotonation of the pyridinium or methylammonium moieties by the chromate anions is clearly shown in the structures of the $[PhNH_2CH_2PyH(CrO_4)]$ and $[PhNH_2(CrO_4)CH_2PyH]$ associations optimized at the BP86/6-31G(d,p) level of theory (Fig. S33).

It can be seen that the CrO_4^{2-} anions deprotonating either the pyridinium or methylammonium moieties are transformed to $HCrO_4^{-}$ species that are associated with the $[PhNHCH_2Py]$ ligand through hydrogen bonds.

The $HCrO_4^{-}$ species interacting with the $[PhNH_2CH_2Py]^{+}$and $PhNH_2CH_2PyH]^{2+}$ ligands yield the $[PhNH_2(HOCrO_3)CH_2Py]$ and $PhNH_2CH_2PyH(HOCrO_3)]^{+}$ weak associations respectively supported by N-H···O-H hydrogen bonds (Fig. S33). The interaction energies for the $[PhNH_2(HOCrO_3)CH_2Py]$ and $PhNH_2CH_2PyH(HOCrO_3)]^{+}$ associations are 11.6 and 23.9 kcal.mol respectively at the BP86/6-31G(d,p) level of theory.

Similarly the deprotonation of the pyridinium or methylammonium moieties of the $[PhNH_2CH_2PyH]^{2+}$ ligand by the $Cr_2O_7^{2-}$ dianions according to the reactions:

$[PhNH_2CH_2PyH]^{2+} + Cr_2O_7^{2-} \rightarrow [PhNH_2CH_2Py]^{+} + HCr_2O_7^{-}$

$[PhNH_2CH_2PyH]^{2+} + Cr_2O_7^{2-} \rightarrow [PhNHCH_2PyH]^{+} + HCr_2O_7^{-}$

are predicted to be slightly exothermic, the estimated exothermicities being -7.1 and -12.8 kcal/mol respectively. Therefore the dichromate anions do not deprotonate the pyridinium or methylammonium moieties of the $[PhNH_2CH_2PyH]^{2+}$ ligand, but interacting with $[PhNH_2CH_2PyH]^{2+}$ ligand yields the weak association $[PhNH_2CH_2PyH(Cr_2O_7)]$ supported by three hydrogen bonds (Fig. S33). The estimated interaction energy amounts to -37.3 kcal/mol.

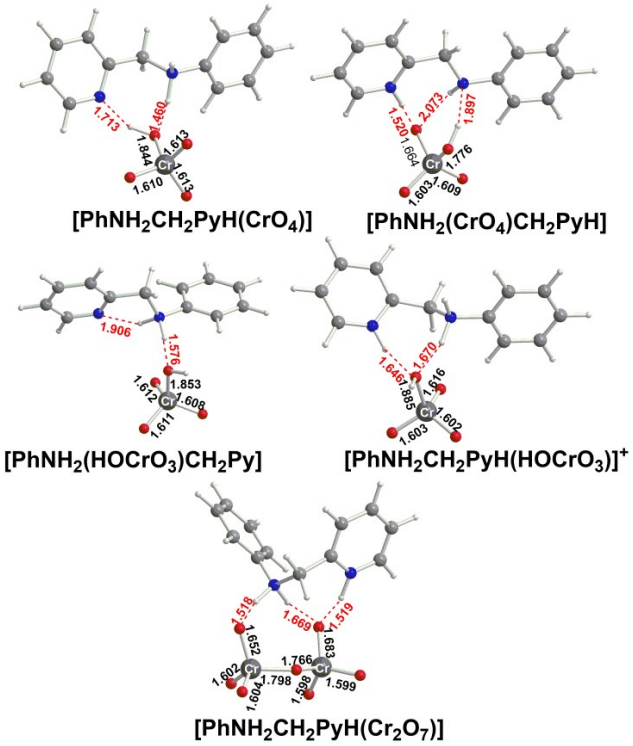

Figure S33. Possible associations of the functional groups of **MOR-2** with chromate and dichromate species optimized at the BP86/6-31G(d,p) level of theory (C, grey; H, white; N, blue; O, red).

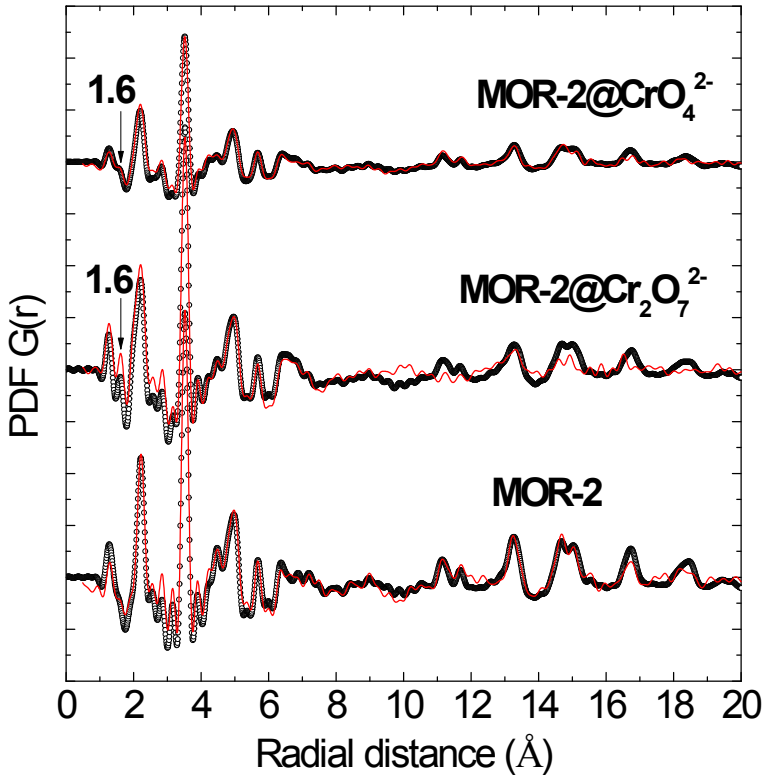

Figure S34. Pair distribution function plots (black dots) of **MOR-2, MOR-2@$Cr_2O_7^{2-}$** and **MOR-2@CrO_4^{2-}.** Red lines represent the fitting of the PDF data using as starting structural models those obtained from Rietveld analysis. The features at ~ 1.6 Å present in the PDF plots of **MOR-2@$Cr_2O_7^{2-}$** and **MOR-2@CrO_4^{2-}** are due to the Cr=O bonds of the Cr(VI) oxoanions.

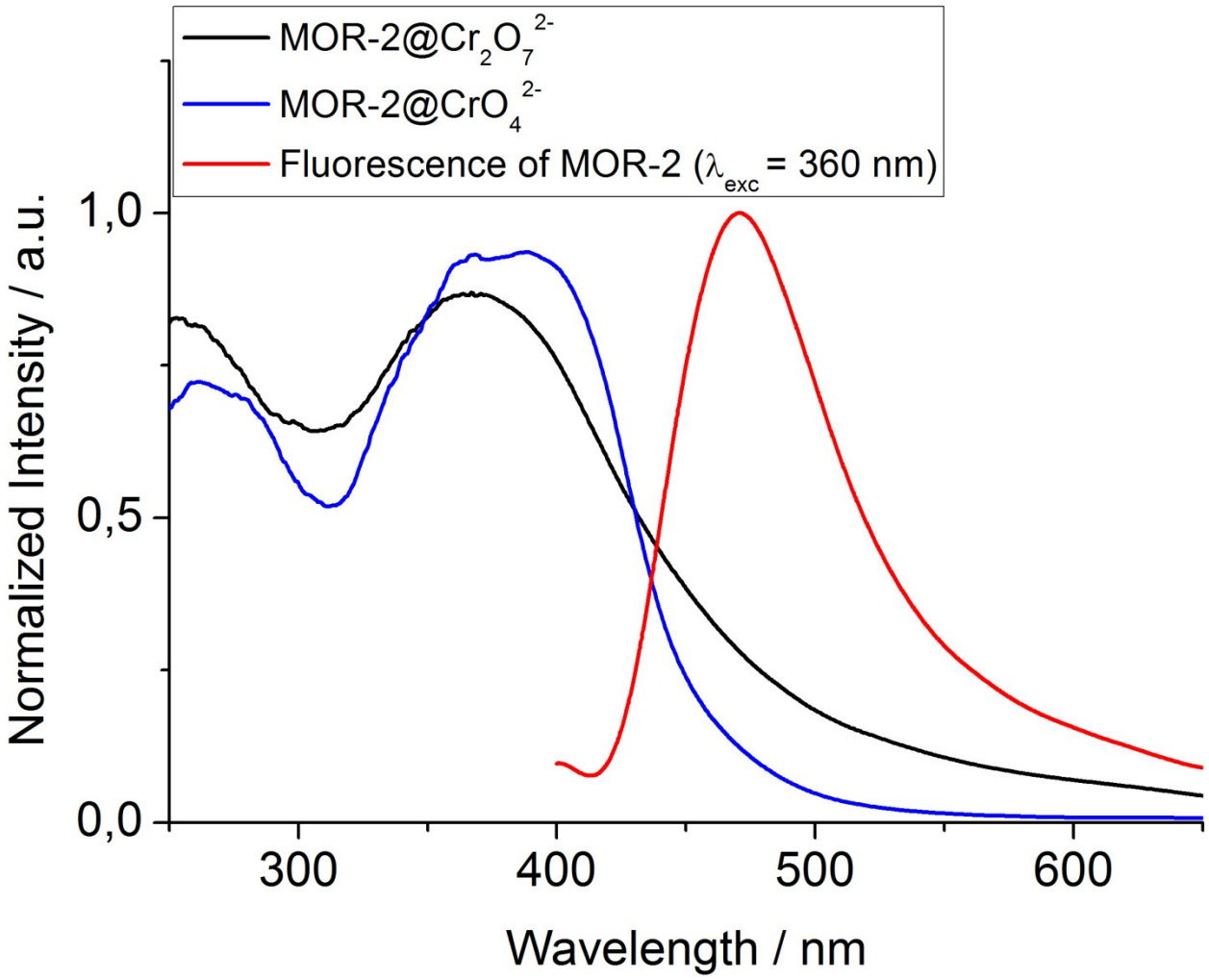

Figure S35. Diffuse reflectance profiles of **MOR-2@$Cr_2O_7^{2-}$** and **MOR-2@CrO_4^{2-}** and fluorescence profile of **MOR-2**. The fluorescence spectrum shows considerable overlap with the low-energy oxido-Cr(VI) based features of the diffuse reflectance spectra.

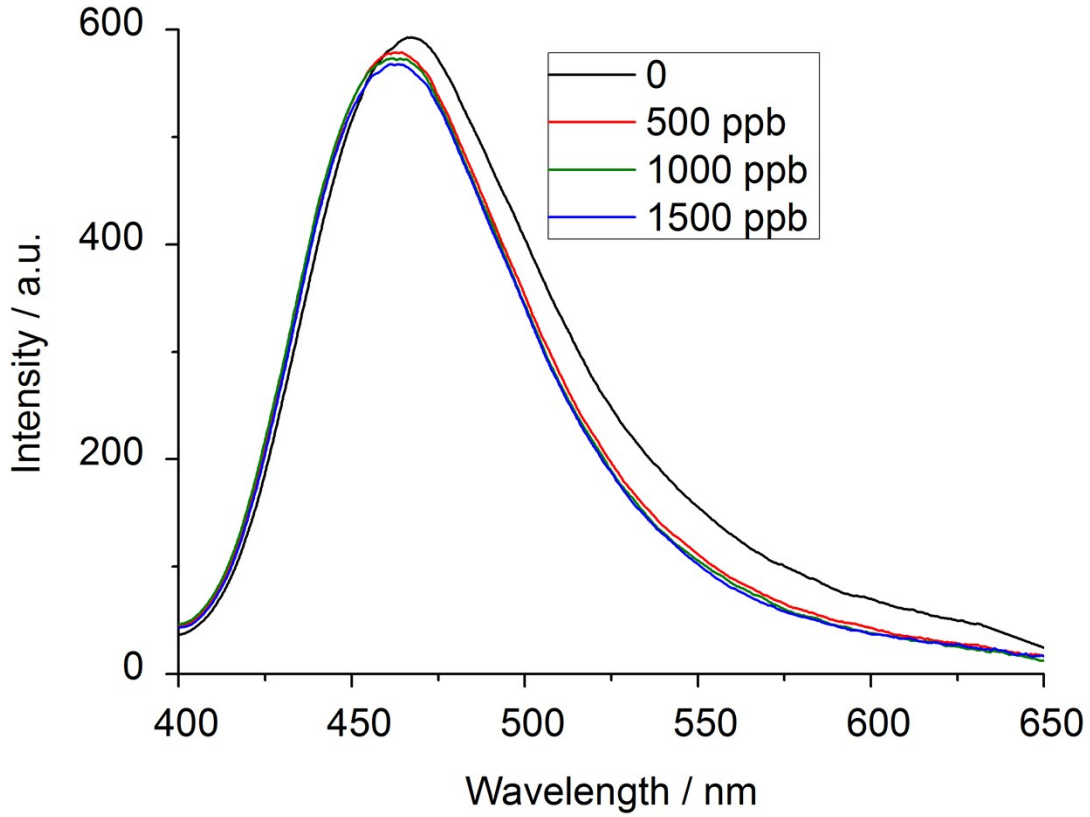

Figure S36. Emission spectra upon excitation at 360 nm of deactivated **MOR-2** suspended in water at pH 3 in the presence of different concentrations of Cr(IV). **MOR-2** was deactivated by treatment for 12 h in methanol with a 100-fold excess of triethylamine in order to deprotonate all the active groups.

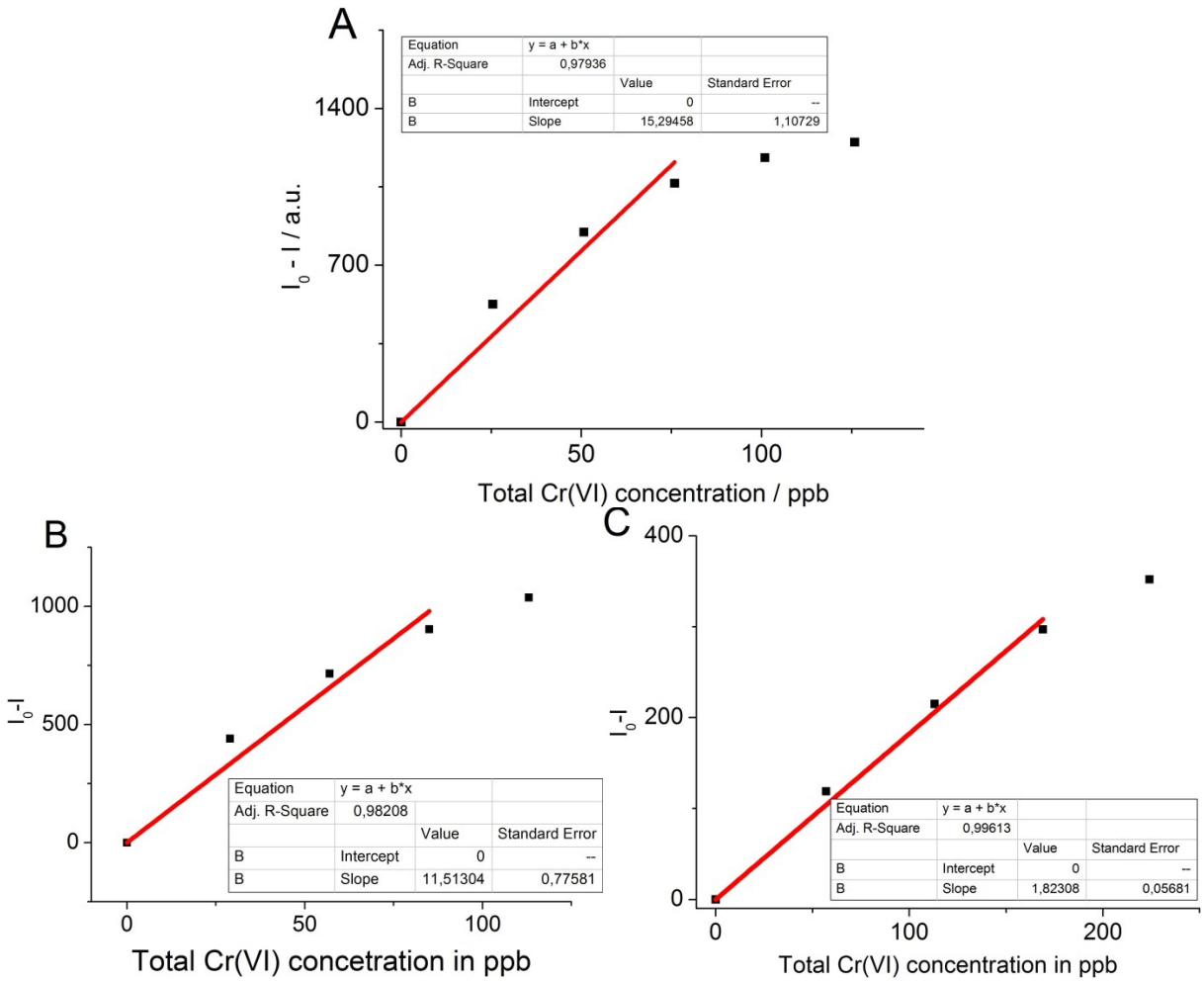

Figure S37. Linear fitting of the initial part of the calibration curves from the data of the fluorescence titrations. The slope of the linear fitting, *S*, in each case was used to determine the limit of detection, LOD, and limit of quantification, LOQ, by using the formulas $LOD = \frac{3S}{SD}$ and $LOQ = \frac{10S}{SD}$ where *SD* is the standard deviation of the measurement of the initial emission intensity I_0. A: Standard dichromate sample and doubly distilled water as solvent, B: Sample from industrial chromium waste and doubly distilled water as solvent and C: Sample from industrial chromium waste and potable water containing 10.5 ppm of competing SO_4^{2-}ions. See main text for more details.

References

1. P. J. Chupas, X. Qiu, J. C. Hanson, P. L. Lee, C. P. Grey and S. J. L. Billinge, *J. Appl. Crystallogr.*, 2003**, 36***,*** 1342.
2. A. P. Hammersley, S. O. Svensson, M. Manfland, A. N. Fitch, and D. Hausermann, *High Pressure Res.*, 1996, **14,** 235.
3. T. Egami and S. J. L. Billinge, *Underneath the Bragg peaks: structural analysis of complex materials* (Pergamon Press, Elsevier, Oxford, England, 2003).
4. X. Qiu, J. W. Thompson and S. J. L. Billinge, *J. Appl. Crystallogr.* **2004**, *37***,** 678.
5. C. L. Farrow, P. Juhas, J. W. Liu, D. Bryndin, E. S. Bozin, J. Bloch, Th. Proffen and S. J. L. Billinge, J. *Phys.: Condens. Matter*, 2007, **19**, 335219.
6. W.W. Wendlandt and H.G. Hecht, *Reflectance Spectroscopy*, Wiley Interscience, New York, 1966.
7. Z. Marczenko and M. Balcerzak, *Separation, Preconcentration and Spectrophotometry in Inorganic Analysis*, 1st Edition, Elsevier, 2000, pg. 159.
8. A. D. Eaton, L. S. Clesceri, A. E. Greenberg, M. A. H. Franson, *Standard methods for the examination of water and wastewater*, American Public Health Association., 20th edition, Washington DC, 1998.
9. R. Soares et al., *Chem. Spec. Bioavailab.*, 2009, **21**, 153.
10. H. E. Taylor, *Inductively Coupled Plasma-Mass Spectroscopy, Practices and Techniques,* Academic Press*,* 2001.
11. *(a)* M. C.Biesinger, C. Brown, J. R. Mycroft, R. D. Davidson and N. S. McIntyre, *Surf. Interface Anal.*, 2004, **36**, 1550; *(b)* E. Desimoni, C. Malitesta, P. G. Zambonin and J. C. Riviere, *Surf. Interface Anal.*, 1988, **13**, 173.
12. A.D. Becke, *Phys. Rev. A*, 1988, **38**, 3098.

13. J. P. Perdew, *Phys. Rev. B,* 1986,**33**, 8822.
14. Frisch, M. J.; Trucks, G. W.; Schlegel, H. B.; Scuseria, G. E.; Robb, M. A.; Cheeseman, J. R.; Scalmani, G.; Barone, V.; Mennucci, B.; Petersson, G. A.; Nakatsuji, H.; Caricato, M.; Li, X.; Hratchian, H. P.; Izmaylov, A. F.; Bloino, J.; Zheng, G.; Sonnenberg, J. L.; Hada, M.; Ehara, M.; Toyota, K.; Fukuda, R.; Hasegawa, J.; Ishida, M.; Nakajima, T.; Honda, Y.; Kitao, O.; Nakai, H.; Vreven, T.; Montgomery, J. A., Jr.; Peralta, J. E.; Ogliaro, F.; Bearpark, M.; Heyd, J. J.; Brothers, E.; Kudin, K. N.; Staroverov, V. N.; Kobayashi, R.; Normand, J.; Raghavachari, K.; Rendell, A.; Burant, J. C.; Iyengar, S. S.; Tomasi, J.; Cossi, M.; Rega, N.; Millam, M. J.; Klene, M.; Knox, J. E.; Cross, J. B.; Bakken, V.; Adamo, C.; Jaramillo, J.; Gomperts, R.; Stratmann, R. E.; Yazyev, O.; Austin, A. J.; Cammi, R.; Pomelli, C.; Ochterski, J. W.; Martin, R. L.; Morokuma, K.; Zakrzewski, V. G.; Voth, G. A.; Salvador, P.; Dannenberg, J. J.; Dapprich, S.; Daniels, A. D.; Farkas, Ö.; Foresman, J. B.; Ortiz, J. V.; Cioslowski, J.; Fox, D. J., Gaussian 09, Revision**D.01**, Gaussian, Inc., Wallingford CT, 2009.
15. J.-D. Chai and M. Martin Head-Gordon, *Phys. Chem. Chem. Phys.*, 2008, **10**, 6615.
16. (a) D. Rappoport and F. Furche, *J. Chem. Phys.*, 2010, **133**, 134105. (b) EMSL basis set exchange, https://bse.pnl.gov/bse/portal, accessed 26-06-2015.

Table S4. Cartesian coordinates and energetic data.

$[PhNH_2CH_2PyH]^{2+}$

N	0.468269000	0.039365000	0.637571000
C	1.932360000	0.021388000	0.348549000
C	2.585759000	-1.215300000	0.300946000
C	3.957551000	-1.227261000	0.004675000
C	4.639548000	-0.023767000	-0.237665000
C	3.956990000	1.202476000	-0.183315000
C	2.585051000	1.236169000	0.110007000
C	-0.391318000	-0.012626000	-0.634867000
C	-1.869415000	0.044158000	-0.336261000
C	-2.561515000	1.237450000	-0.121715000
C	-3.900965000	-1.193575000	-0.022302000
C	-3.938598000	1.207317000	0.158723000
C	-4.614786000	-0.019307000	0.210350000
N	-2.572645000	-1.126654000	-0.280393000
H	0.230952000	0.887772000	1.181222000
H	0.236696000	-0.756805000	1.255554000
H	2.049255000	-2.149158000	0.495859000
H	4.489336000	-2.181636000	-0.032062000
H	5.708801000	-0.041076000	-0.466506000
H	4.488723000	2.140138000	-0.365184000
H	2.049789000	2.189000000	0.157672000
H	-0.100667000	-0.927348000	-1.169725000
H	-0.093652000	0.856136000	-1.237452000
H	-2.024703000	2.186667000	-0.181801000
H	-4.343631000	-2.189687000	-0.016190000
H	-4.478317000	2.142004000	0.328313000
H	-5.683901000	-0.076447000	0.419544000
H	-2.082019000	-2.011268000	-0.452241000

Sum of electronic and zero-point Energies= -574.656887
Sum of electronic and thermal Energies= -574.645005
Sum of electronic and thermal Enthalpies= -574.644060
Sum of electronic and thermal Free Energies= -574.696770

$[PhNH_2CH_2Py]^+$

N	-0.425201000	-0.691884000	0.787792000
C	-1.751479000	-0.218576000	0.345127000
C	-1.842572000	1.039094000	-0.266875000
C	-3.101506000	1.486931000	-0.695141000
C	-4.239782000	0.684976000	-0.508493000
C	-4.124607000	-0.571436000	0.107913000
C	-2.871745000	-1.035388000	0.539382000
C	0.478629000	-1.276024000	-0.286283000
C	1.823382000	-0.562957000	-0.168982000
C	2.950277000	-0.935096000	-0.915765000
C	2.959425000	1.186030000	0.858167000
C	4.123486000	-0.186822000	-0.747708000
C	4.131706000	0.892293000	0.152138000
N	1.826720000	0.469009000	0.696609000
H	-0.529027000	-1.362315000	1.563926000
H	0.201956000	0.115036000	1.148826000
H	-0.951847000	1.659891000	-0.402244000
H	-3.189402000	2.468092000	-1.170004000
H	-5.218727000	1.041310000	-0.841954000
H	-5.009124000	-1.197076000	0.256545000
H	-2.774311000	-2.014736000	1.017780000
H	0.008911000	-1.085919000	-1.263227000
H	0.563243000	-2.362651000	-0.144265000
H	2.908937000	-1.782067000	-1.606011000
H	2.913087000	2.012734000	1.574115000
H	5.023996000	-0.444578000	-1.312354000
H	5.030385000	1.494248000	0.307182000

Sum of electronic and zero-point Energies= -574.243461
Sum of electronic and thermal Energies= -574.231874
Sum of electronic and thermal Enthalpies= -574.230930
Sum of electronic and thermal Free Energies= -574.283161

[PhNHCH$_2$PyH]$^+$

N	0.524044000	-1.349761000	-0.040024000
C	1.671214000	-0.517396000	0.007879000
C	1.627525000	0.776749000	0.571216000
C	2.776873000	1.583469000	0.565406000
C	3.975372000	1.125582000	-0.003370000
C	4.014489000	-0.159860000	-0.572041000
C	2.877570000	-0.977750000	-0.566967000
C	-0.516336000	-1.233736000	0.977880000
C	-1.730097000	-0.478003000	0.455253000
C	-2.823493000	-0.052860000	1.217269000
C	-2.744541000	0.398548000	-1.532024000
C	-3.885546000	0.602818000	0.580676000
C	-3.849500000	0.831751000	-0.808229000
N	-1.739617000	-0.234479000	-0.876500000
H	0.746678000	-2.317709000	-0.273975000
H	0.701456000	1.166000000	1.004779000
H	2.725569000	2.582888000	1.009489000
H	4.866635000	1.759941000	-0.004759000
H	4.940842000	-0.536446000	-1.017920000
H	2.918943000	-1.981530000	-1.004689000
H	-0.151156000	-0.739676000	1.896749000
H	-0.853596000	-2.241389000	1.276287000
H	-2.833005000	-0.237455000	2.293711000
H	-2.621185000	0.532181000	-2.607142000
H	-4.744675000	0.939935000	1.166498000
H	-4.665188000	1.341852000	-1.322827000
H	-0.883481000	-0.574792000	-1.358219000

Sum of electronic and zero-point Energies= -574.252633
Sum of electronic and thermal Energies= -574.240988
Sum of electronic and thermal Enthalpies= -574.240043
Sum of electronic and thermal Free Energies= -574.291862

[PhNHCH$_2$Py]

N	0.431486000	0.215747000	-0.356168000
C	1.798042000	0.118426000	-0.150412000
C	2.589588000	1.299403000	-0.111841000
C	3.975449000	1.225156000	0.058186000
C	4.622018000	-0.018762000	0.195646000
C	3.846891000	-1.188901000	0.158309000
C	2.454376000	-1.133019000	-0.010802000
C	-0.477820000	-0.884159000	-0.104952000
C	-1.915420000	-0.382511000	-0.039397000
C	-2.991957000	-1.290212000	-0.025873000
C	-3.353866000	1.426235000	0.113870000
C	-4.295308000	-0.788743000	0.068179000
C	-4.485207000	0.601713000	0.140216000
N	-2.089684000	0.954327000	0.027995000
H	-0.016950000	1.123796000	-0.194103000
H	2.098142000	2.273584000	-0.217044000
H	4.558703000	2.152299000	0.087056000
H	5.706758000	-0.071248000	0.329086000
H	4.327949000	-2.167817000	0.263569000
H	1.876596000	-2.061436000	-0.042122000
H	-0.242969000	-1.405675000	0.851244000
H	-0.402916000	-1.658664000	-0.895204000
H	-2.804862000	-2.367028000	-0.088269000
H	-3.456898000	2.517182000	0.162893000
H	-5.151232000	-1.470515000	0.081695000
H	-5.485644000	1.037250000	0.211631000

Sum of electronic and zero-point Energies= -573.811952
Sum of electronic and thermal Energies= -573.800178
Sum of electronic and thermal Enthalpies= -573.799234
Sum of electronic and thermal Free Energies= -573.851250

[$PhNH_2CH_2PyH(CrO_4^{2-})$]

O	1.692325000	-3.426816000	-0.486408000
Cr	0.489194000	-2.431179000	-0.125166000
O	0.847954000	-1.448578000	1.168360000
O	0.259721000	-1.327329000	-1.496800000
O	-0.857262000	-3.257126000	0.179934000
N	-0.713404000	0.803944000	0.126882000
C	-2.137953000	0.932026000	0.102826000
C	-2.910581000	-0.206715000	0.433527000
C	-4.308161000	-0.150475000	0.382281000
C	-4.965626000	1.032952000	-0.000334000
C	-4.200317000	2.160764000	-0.328280000
C	-2.795925000	2.120870000	-0.275902000
C	0.075321000	2.037623000	0.127036000
C	1.579177000	1.856375000	0.087993000
C	2.406013000	2.924633000	-0.295276000
C	3.515552000	0.519710000	0.482275000
C	3.797048000	2.777916000	-0.281038000
C	4.366021000	1.554296000	0.113618000
N	2.167492000	0.692233000	0.465286000
H	-0.206581000	-0.507772000	-1.147093000
H	-0.429957000	0.157363000	0.879994000
H	-2.409276000	-1.138478000	0.719756000
H	-4.887769000	-1.041731000	0.644196000
H	-6.058305000	1.073178000	-0.038634000
H	-4.692687000	3.093242000	-0.622936000
H	-2.232881000	3.023218000	-0.526393000
H	-0.158390000	2.681941000	1.003032000
H	-0.187949000	2.626935000	-0.766773000
H	1.945117000	3.865534000	-0.604980000
H	3.860439000	-0.467456000	0.795133000
H	4.435859000	3.611909000	-0.583087000
H	5.446506000	1.402976000	0.132316000
H	1.591281000	-0.186846000	0.761233000

Sum of electronic and zero-point Energies= -1920.603266
Sum of electronic and thermal Energies= -1920.584885
Sum of electronic and thermal Enthalpies= -1920.583941
Sum of electronic and thermal Free Energies= -1920.651752

[$PhNH_2(CrO_4^{2-})CH_2PyH$]

O	-2.445152000	2.694324000	-0.272005000
Cr	-0.841584000	2.585050000	-0.181760000
O	-0.213113000	3.883932000	0.538422000
O	-0.426869000	1.102326000	0.832504000
O	-0.199802000	2.384159000	-1.647966000
N	0.805726000	-0.858140000	-0.283113000
C	2.271714000	-0.795863000	-0.137332000
C	2.802637000	-0.025496000	0.907007000
C	4.196339000	0.028161000	1.064611000
C	5.035115000	-0.678706000	0.187219000
C	4.483708000	-1.443470000	-0.854302000
C	3.091651000	-1.510196000	-1.021868000
C	0.171094000	-2.000476000	0.497847000
C	-1.329104000	-2.086492000	0.283099000
C	-1.914501000	-3.263300000	-0.209763000
C	-3.408487000	-1.058649000	0.472683000
C	-3.310141000	-3.322159000	-0.345660000
C	-4.073382000	-2.200444000	0.002413000
N	-2.069030000	-0.999721000	0.620693000
H	0.557158000	-0.953520000	-1.279477000
H	0.339960000	0.096320000	0.103317000
H	2.135713000	0.528081000	1.574570000
H	4.623935000	0.629016000	1.872365000
H	6.120814000	-0.631055000	0.312925000
H	5.135362000	-1.990979000	-1.541213000
H	2.655358000	-2.105533000	-1.830649000
H	0.406608000	-1.808618000	1.556778000
H	0.664762000	-2.933780000	0.192726000
H	-1.287128000	-4.117805000	-0.477744000
H	-3.961166000	-0.154004000	0.745101000
H	-3.789508000	-4.229995000	-0.722647000
H	-5.162181000	-2.200467000	-0.090720000
H	-1.218905000	0.460781000	0.900500000

Sum of electronic and zero-point Energies= -1920.600674

Sum of electronic and thermal Energies= -1920.582174

Sum of electronic and thermal Enthalpies= -1920.581229

Sum of electronic and thermal Free Energies= -1920.651674

[$PhNH_2CH_2Py(HOCrO_3^-)$]

O	0.908628000	3.893650000	0.237996000
Cr	1.484085000	2.396023000	0.088105000
O	1.112900000	1.504357000	1.378767000
O	0.645252000	1.533347000	-1.321015000
O	3.070589000	2.419881000	-0.170582000
H	1.166902000	1.571788000	-2.146050000
N	-0.148108000	-0.784443000	-0.294851000
C	0.959086000	-1.724683000	-0.066980000
C	0.846096000	-2.686918000	0.947583000
C	1.903270000	-3.587643000	1.147471000
C	3.051808000	-3.522258000	0.340506000
C	3.148666000	-2.550778000	-0.668635000
C	2.097925000	-1.643387000	-0.879329000
C	-1.325837000	-1.329717000	-1.066712000
C	-2.599174000	-0.725557000	-0.487182000
C	-3.822864000	-0.769167000	-1.174237000
C	-3.558392000	0.334685000	1.338018000
C	-4.953775000	-0.232513000	-0.544131000
C	-4.823151000	0.329720000	0.736126000
N	-2.464367000	-0.184998000	0.740780000
H	0.211126000	0.118375000	-0.779747000
H	-0.581810000	-0.453303000	0.609274000
H	-0.049469000	-2.730458000	1.575362000
H	1.827477000	-4.339130000	1.938662000
H	3.872902000	-4.227081000	0.501310000
H	4.042953000	-2.493557000	-1.295843000
H	2.167177000	-0.877027000	-1.656260000
H	-1.331772000	-2.426094000	-0.952437000
H	-1.199437000	-1.094826000	-2.133791000
H	-3.885872000	-1.210460000	-2.173115000
H	-3.405986000	0.768813000	2.332151000
H	-5.924248000	-0.247884000	-1.048691000
H	-5.681542000	0.761797000	1.256830000

Sum of electronic and zero-point Energies= -1920.597299

Sum of electronic and thermal Energies= -1920.578270

Sum of electronic and thermal Enthalpies= -1920.577325

Sum of electronic and thermal Free Energies= -1920.649632

[$PhNH_2CH_2PyH(HOCrO_3^-)$]

O	-1.386096000	3.588393000	0.278172000
Cr	-0.128695000	2.624296000	0.034427000
O	0.296952000	1.859076000	1.392770000
O	-0.599139000	1.215104000	-1.126387000
O	1.098508000	3.443767000	-0.590014000
H	-0.697038000	1.490626000	-2.060513000
N	0.545054000	-1.153071000	-0.550439000
C	2.002658000	-1.265450000	-0.286128000
C	2.630598000	-0.288560000	0.497933000
C	4.008727000	-0.414627000	0.734144000
C	4.729505000	-1.492270000	0.193480000
C	4.075391000	-2.457419000	-0.588859000
C	2.697133000	-2.351701000	-0.832496000
C	-0.323597000	-1.345328000	0.692406000
C	-1.787443000	-1.535436000	0.365754000
C	-2.505666000	-2.665813000	0.763512000
C	-3.763355000	-0.605772000	-0.603184000
C	-3.878690000	-2.752623000	0.478171000
C	-4.516599000	-1.711860000	-0.211395000
N	-2.445597000	-0.544592000	-0.303207000
H	0.284501000	-1.854264000	-1.263131000
H	0.290110000	-0.187349000	-0.948194000
H	2.059749000	0.548999000	0.916053000
H	4.517750000	0.338319000	1.342495000
H	5.803489000	-1.579825000	0.381629000
H	4.632634000	-3.297165000	-1.013029000
H	2.181503000	-3.100149000	-1.442480000
H	-0.171152000	-0.442463000	1.309138000
H	0.054893000	-2.224305000	1.229205000
H	-1.991181000	-3.469011000	1.294652000
H	-4.172750000	0.243218000	-1.152363000
H	-4.443414000	-3.634587000	0.790376000
H	-5.580321000	-1.750863000	-0.451100000
H	-1.870071000	0.289800000	-0.639815000

Sum of electronic and zero-point Energies= -1921.029545
Sum of electronic and thermal Energies= -1921.011024
Sum of electronic and thermal Enthalpies= -1921.010080
Sum of electronic and thermal Free Energies= -1921.077750

[$PhNH_2CH_2PyH(Cr_2O_7^{2-})$]

N	0.678852000	-0.854221000	-0.270298000
C	1.763880000	-1.671725000	0.293207000
C	2.251030000	-2.765659000	-0.437705000
C	3.281223000	-3.542009000	0.113950000
C	3.808574000	-3.225722000	1.377564000
C	3.303349000	-2.132007000	2.098318000
C	2.273914000	-1.345096000	1.557672000
C	1.049615000	0.032187000	-1.440175000
C	2.042115000	1.123270000	-1.103700000
C	3.242747000	1.296584000	-1.797439000
C	2.509653000	3.051289000	0.217869000
C	4.079986000	2.377777000	-1.476340000
C	3.710525000	3.267830000	-0.457789000
N	1.716485000	2.009643000	-0.120663000
H	0.245894000	-0.222416000	0.472958000
H	-0.174933000	-1.454402000	-0.625289000
H	1.829728000	-3.015446000	-1.416172000
H	3.667040000	-4.399159000	-0.445196000
H	4.611034000	-3.836059000	1.802132000
H	3.706846000	-1.886363000	3.084765000
H	1.867949000	-0.494945000	2.114473000
H	0.101121000	0.467672000	-1.796882000
H	1.457386000	-0.603336000	-2.237455000
H	3.513145000	0.590560000	-2.585217000
H	2.150946000	3.686481000	1.029454000
H	5.018408000	2.519011000	-2.018576000
H	4.339742000	4.115675000	-0.181980000
H	0.792384000	1.824749000	0.439620000
O	-4.048067000	-1.375916000	-1.765935000
O	-3.288680000	-1.828526000	0.707794000
O	-1.480422000	-1.897200000	-1.260950000
Cr	-2.864164000	-1.191415000	-0.699977000
O	-2.545059000	0.566963000	-0.505927000
O	-2.113211000	3.073159000	0.448488000
O	-0.364047000	1.165773000	1.170685000
O	-2.861570000	1.245450000	2.157988000
Cr	-1.976890000	1.534002000	0.858742000

Sum of electronic and zero-point Energies= -3190.988670
Sum of electronic and thermal Energies= -3190.965701
Sum of electronic and thermal Enthalpies= -3190.964757
Sum of electronic and thermal Free Energies= -3191.044597